MODELING FLUID FLOW AND HEAT TRANSFER IN A POROUS CERAMIC USED FOR HIGH CONCENTRATION SOLAR RECEIVERS

BY

MAJID TAREQ LINJAWI

A Thesis Presented to the
DEANSHIP OF GRADUATE STUDIES

KING FAHD UNIVERSITY OF PETROLEUM & MINERALS
DHAHRAN, SAUDI ARABIA

In Partial Fulfillment of the
Requirements for the Degree of

MASTER OF SCIENCE

In

MECHANICAL ENGINEERING

MAY 2018

KING FAHD UNIVERSITY OF PETROLEUM & MINERALS
DHAHRAN 31261, SAUDI ARABIA

DEANSHIP OF GRADUATE STUDIES

This thesis, written by **MAJID TAREQ LINJAWI** under the direction of his thesis adviser and approved by his thesis committee, has been presented to and accepted by the Dean of Graduate Studies, in partial fulfillment of the requirements for the degree of **MASTER OF SCIENCE IN MECHANICAL ENGINEERING**.

Thesis Committee

R.B. Mansour
Dr.Rached Ben-Mansour (Adviser)

Dr.Esmail Mokheimer (Member)

M Antar
Dr.Mohammed A. Antar (Member)

Dr.Zuhair Gasem
Department Chairman

Dr. Salam A. Zummo
Dean of Graduate Studies

23/5/18
Date

My mother who taught me the alphabets . . .
My father who taught me how to live life . . .

ACKNOWLEDGMENTS

First of all, I thank Allah for giving me all what I have in life. My life is full of his grace and blessings.

Second, I would like to take the chance to thank my parents who always encouraged me to thrive for knowledge and seek the best and my wife who supported me all the way through my Master's degree.

Many thanks to my uncle Professor Amro Al-Qutub for his support and guidance.

Special thanks to my advisor Dr. Rached Ben-Mansour for teaching me three graduate courses, accepting to be my advisor, for his efforts and patience.

I also thank Prof. Esmail Mokheimer and Prof. Mohammed Antar for accepting to be in the committee of my defense. I extend my thanks to all the great faculty members who taught me at KFUPM.

Finally I really thank my friends Hamad Al-Mahmoud, Azzam Al-Farraj, Ahmad Abo-Elyaman and Ghazi Zul-Hazmi for their help at different stages in my way to my Master's degree.

TABLE OF CONTENTS

LIST OF TABLES

LIST OF FIGURES

THESIS ABSTRACT

NAME: Majid Tareq Linjawi

TITLE OF STUDY: Modeling Fluid Flow and Heat Transfer in a Porous Ceramic Used for High Concentration Solar Receivers

MAJOR FIELD: Mechanical Engineering

DATE OF DEGREE: May, 2018

This thesis investigates the fluid flow and the heat transfer in ceramic foams, used for high concentration solar receivers; numerically utilizing a simplified geometrical model. The simplified geometry is a truncated octahedron strut consisting of cylindrical beams; ligaments. Three configuration of the geometry are constructed; a basic geometry consisting of a single cell model, two multiple unit cells geometries of 2 by 2 by 2 cells and a 2 by 2 by 3 cells. This novel approach has not been previously used in the literature to study ceramic foams as concentrated solar absorbers. The fluid flow and heat transfer equations within the simplified models are solved numerically using a commercial CFD program. A basic case with an irradiation of $G = 2\,MW/m^2$ and an air mass flux of $m'' = 12.5\,kg/m^2 \cdot s$

is conducted for the three geometric configurations. The radiation, temperature and velocity profiles are reported. The cell efficiency is found to be $\eta = 93.1\%$ at air exit temperature of $T_{g,out} = 447\ K$ for $2^2 \times 3$ multiple unit cells case. Further, a parametric study consisting of more than 500 design points is conducted. A pressure drop and volumetric heat transfer coefficient relations are derived against superficial air velocity. The relations are found to be consistent with published references. The ratio of the solar flux to the mass flux is identified as a key parameter that affect most critical performance parameters of a unit cell. The parametric study showed that the surface absorbtivity of the foam material have a much larger effect on the foam performance than its thermal conductivity. The unit cell simplified method proved to be a simple, robust and accurate method in modeling fluid flow and heat transfer in ceramic foams.

ملخص الرسالة

الاسم الكامل: ماجد بن طارق بن عبدالله لنجاوي

عنوان الرسالة: محاكاة حركة الموائع وانتقال الحرارة في السيراميكيات الإسفنجية المستخدمة كمستقبلات لأشعة الشمس عالية التركيز

التخصص: هندسة ميكانيكية

تاريخ الدرجة العلمية: رمضان 1439 هـ , الموافق مايو 2018

تبحث هذه الرسالة حركة الموائع وانتقال الحرارة في السيراميكيات الإسفنجية المستخدمة كمستقبلات لأشعة الشمس عالية التركيز باستخدام برامج المحاكاة الإلكترونية وافتراض شكل مبسط للإسفنج. تم اختيار الشكل المبسط بناء على أبحاث سابقة أثبتت تشابه النتائج المحصلة منه مع النتائج المحصلة من الاختبارات المعملية. قمنا بعرض عملية محاكاة واحدة بالتفصيل وذلك تحت الظروف الآتية : شدة الإشعاع الشمسي: ألفي شمس, معدل تدفق الهواء: 12.5 كيلوجرام في المتر المربع خلال الثانية, معامل التوصيل الحراري: 100 واط في المتر لكل درجة حرارة و معامل امتصاص الأشعة ب 0.9 وحصلنا على كفاءة تعادل 93.1 % ودرجة حرارة للهواء الخارج تعادل 447 كيلفن. ثم تم عمل دراسة موسعة لمعرفة تأثير العوامل المختلفة على الأداء. استخلصت العلاقة بين سرعة حركة الهواء في الإسفنج وبين معامل الاحتكاك ومعامل انتقال الحرارة ووجدت العلاقة مقاربة لما تم استخلاصه من دراسات سابقة. حددت النسبة بين شدة الإشعاع و معدل تدفق الهواء كأهم نسبة تتحكم في أداء المستقبلات الشمسية. ووجد أن لمعامل امتصاص الأشعة أثر كبير على النتائج بينما ليس لمعامل التوصيل الحراري للمكون الصلب للإسفنج أثر ملاحظ. الخلاصة: تم إثبات أن الطريقة المستخدمة في هذا البحث بسيطة وغير مكلفة وتؤتي نتائج دقيقة إلى حد بعيد.

CHAPTER 1

INTRODUCTION

This chapter presents the background of the problem studied in the thesis, explains the motivation for the research and shows its possible range of influence.

1.1 Background

In a world of increasing awareness of the dangers of global warming and fossil fuels emissions; many innovative clean energy generation methods are developed. Solar energy is one of the most promising technologies being proposed. Although solar photovoltaic PV leads the worldwide market in terms of total installed capacity by 50 GW installed in 2015, concentrated solar power is showing a promising future in developing countries with more than 500 MW capacity installed in the last two years [7].

In many concentrated solar receivers, ceramics foams are used as absorbers. A typical arrangement of a parabolic dish with a concentrated solar reciever utilizing ceramic foam absorber is shown in Fig.1.1. In such absorbers, solar radiation

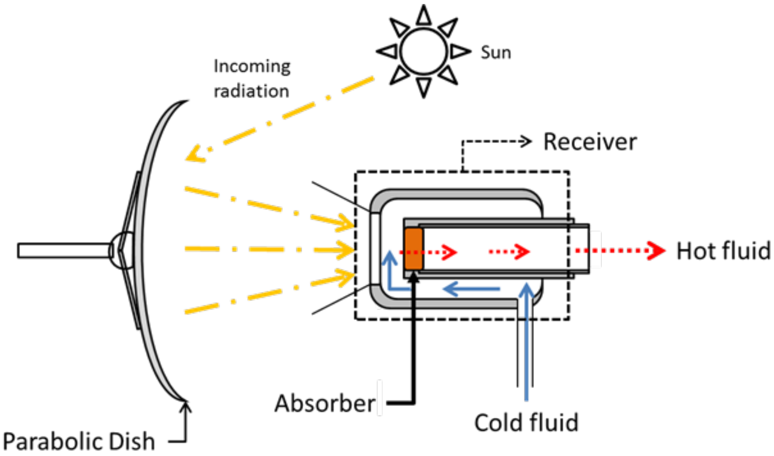

Figure 1.1: Schematic diagram of a solar solar dish [1].

penetrates through the ceramic foam while its intensity decays slowly due to the absorption and scattering of the solar radiation by the solid ligaments of the foam. The absorbed fraction of the radiation causes an increase in the temperature of the material, therefore a stream of fluid - usually air - is forced through the ceramic foam to carry away the absorbed energy. The fluid, which has been heated by the ceramic foam, can be then used in a power generation cycle, or steam reforming process.

1.2 Motivation

However, deep understanding of the behavior of fluid flow and heat transfer within a ceramic foams used as absorbers in concentrated solar receiver has not been achieved. Adequate understanding of the problem is required in order to increase the efficiency and lifetime, and reduce costs and losses for such systems. The lack of concrete knowledge in the area is apparent. For example, there are no complete published design, operation or optimization guidelines for such systems. These problems were faced during the design of a $20\,kW$ solar dish to be built for research purposes at King Fahd University of Petroleum and Minerals and was the main motivator for this research.

CHAPTER 2

LITERATURE REVIEW

This chapter presents and compares the methods used in the literature to develop a better understanding of the fluid flow and heat transfer phenomena in ceramic foams used in concentrated solar receivers. The chapter concludes with identifying the main knowledge gaps in literature.

There are many methods that can be used to develop a better understanding of the heat transfer and fluid flow and heat transfer phenomena in ceramic foams used in concentrated solar receivers. Experimental methods, detailed modeling, and simplified modeling are the three main methods used in the literature. Each method has its own advantages and drawbacks. For example; at least four separate experimental setups are needed to determine the thermo-physical properties of fluid flow and heat transfer in ceramic foams using experimental methods. Additionally, it is very difficult to simulate the concentrated sun irradiation inside a lab, which is required to obtain the properties of ceramic foams under high irradiation and temperatures. In many cases, researches had to construct actual solar concentrators and receivers to obtain the fluid flow and heat transfer characteristics of such foams. Therefore, experimental methods are considered expensive and time consuming methods. Detailed modeling can be used to produce accurate simulations and results given the proper inputs are provided correctly. However, this method requires supercomputers and expensive equipment to achieve. Simplified models on the other hand can be used without the expensive computers and equipment but the simplified models results need to be validated and their accuracy has to be tested.

The following sections presents the three main methods used in the literature to study the behavior of fluid flow and heat transfer through ceramic foams.

2.1 Experimental Methods

2.1.1 Pressure Drop

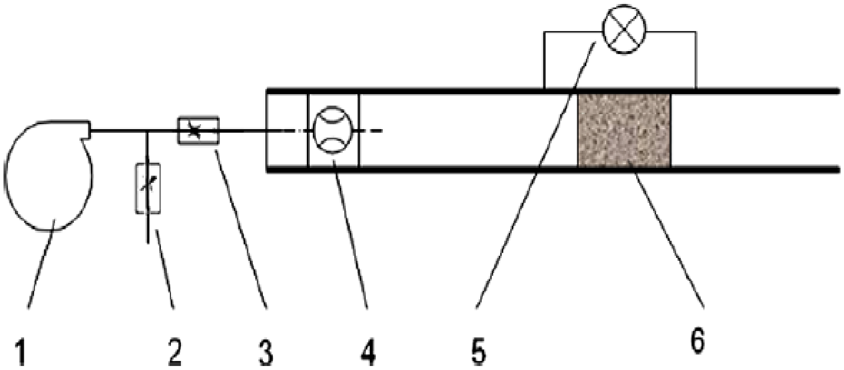

(1) Compressor, (2) by-pass valve, (3) throttle, (4) volumetric meter, (5) pressure drop meter (6) specimen

Figure 2.1: Experimental setup for measuring pressure drop [2]

Using an experimental setup is the easiest way to determine pressure drop for a flow through porous media including ceramic foams. Various researchers have reported their setup and results [2, 8]. Mostly the results are in form of modified Darcy-Forchheimer equation:

$$-\nabla P = \frac{\eta}{K_1}u + \frac{\rho}{K_2}|u|u \qquad (2.1)$$

Where $K_1 \& K_2$ are experimentally determined constants called the specific permeability and the form drag respectively. K_2 can be defined as $1/\beta$ where β is the inertial coefficient. This form of equation is also recommended by the manufacturer of the ceramic foam samples to be used in the proposed solar absorber. A detailed procedure on how to obtain $K_1 \& K_2$ factors is provided in Fluent manual [9].

Since the experimental setup to measure pressure drop across the foams is very simple and give accurate results, other methods were rarely used in determining pressure drop across ceramic foams.

2.1.2 Volumetric Heat Transfer Coefficient

In 1993 Younis and Viskanta used a transient method by inserting a cold sponge sample into a hot gas stream and recording the temperature of the gas outlet during the sponge heating-up process they determined the volumetric heat transfer coefficient h_v [3]. The foam specimens used were made of Al_2O_3 with porosity of 92 % with different pore diameters. The authors correlated the experimental values using a Nusselt approach with two fitting parameters given by:

$$Nu = C.Re^{m} \tag{2.2}$$

A schematic representation of their experimental setup is shown in Fig.2.2.

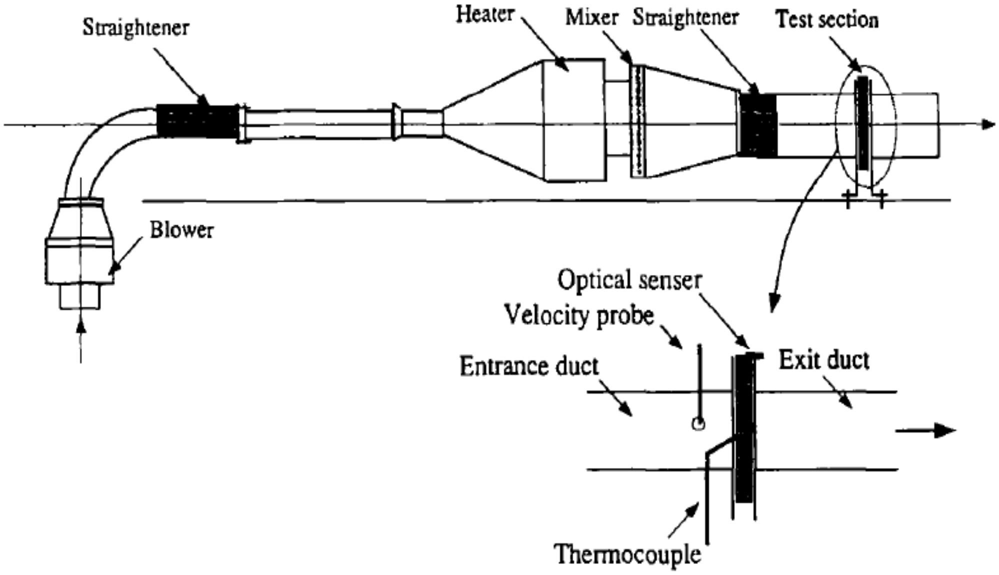

Figure 2.2: Schematic diagram of test apparatus used by Younis and Viskanta to measure volumetric heat transfer coefficient [3]

Recently, Dietrich reviewed the work done in determination of the heat transfer coefficients for solid ceramics and further examined three different porous ceramics made of $Al_2O_3, OBSiC, and Mullite$ [10]. His final conclusion was a proposed general correlation in form of:

$$Nu = 0.57 * C_{Re} * C_{Geo} * Re^{\frac{2}{3}} Pr^{\frac{1}{3}} \tag{2.3}$$

90% of his data fits in the ±40% of the proposed correlation with OB SiC best fitting the correlation.

In most of the studies reviewed, maximum temperature difference between the porous media and the cooling air was $100°C$ and air was the heating the porous media. However for more appropriate results the porous media should be used to heat the passing air, which is similar to the case of solar absorbers. This approach was applied on metal foam by Brendelberger [11]. Experimental results has not been validated under operation conditions of an actual solar receiver where porous ceramic temperature rise up to $1500°C$.

Clearly in the literature there is a gap in the adequate validated measurements of volumetric heat transfer coefficient for ceramics foams used as volumetric solar receivers.

2.1.3 Thermal Diffusivity

Due to the nature of porous media which acts like semi-transparent material, thermal diffusivity happens by conduction and radiation. However, at relatively low temperatures, conduction is the dominant contributor to the thermal conductivity [12]. Therefore, many experimental references which study thermal diffusivity using traditional methods of measuring thermal conductivity neglects the effect of radiation, therefore their results are accurate only within the range below $200°C$ [12]. However, the temperature of the ceramic foam reaches temperatures up to $1500°C$ when used as solar abrorbers. Hence thermal diffusivity measurements neglecting the radiation are not adequate. Therefore only experimental studies on evaluation of thermal diffusivity at high temperatures will be considered in this review.

In 2009 R. Coquard and colleagues proposed an effective thermal conductivity identification method using thermograms obtained from laser-FLASH measurements [13]. Their method permits to evaluate, at ambient and high temperatures, the effective thermal conductivity and two global radiative properties of various metal or ceramic foams, describing the thermal behavior of their equivalent homogeneous semi-transparent materials. Thier method is promising since conduction and radiation contributions to heat transfer can be evaluated from a unique experiment [13]. However, their model requires a prior knowledge of the thermal conductivity, extinction coefficient, and scattering albedo. Their results were only validated up to 700 K, which is lower than the required range in volumetric solar absorbers.

In the institute of thermal process engineering at Karlsruhe, two experimental setups were built to measure both axial and radial two-phase (solid and air) thermal conductivity for ceramic sponges. By heating a foam from one direction and blowing cooling air through the sponge, measuring the temperatures at different locations, and applying the steady state energy balance, effective two phase thermal conductivity could be obtained. However, their model neglects radiation and is only limited to temperatures below $200°C$.[14, 15]

2.1.4 Radiation Properties

There are three main properties that determines a porous material radiation behavior; absorption coefficient, scattering coefficient, and scattering phase function [16]. Each of the three properties can be spectral, directional and temperature dependent or independent. However, these properties cannot be directly measured using a singlw setup, rather it should be derived from other measurable quantities such as transmissivity, and reflectivity [4]. The derivation of the defining properties from measurable quantities is done by inverse radiative analysis method.

A relatively complex setup made of a radiation source and group of mirrors and reflectors combined with detectors and sensors are required to accurately determine the spectral directional transmissivity and reflectivity. Figure 2.3 shows the experimental setup used by Hendricks to measure radiative properties at infrared region of Oxide bonded Silicone Carbide and Zirconium oxide foams [4].

The obtained results in form of transmissivity, and reflectivity were then analyzed and studied. Using a systematic trial and error approach, a well matching values of absorption coefficient,scattering coefficient, and scattering phase function was obtained. The detailed mathematical derivation of the inverse radiative problem is shown his work [4].

Similar approach was also used by other researchers for different materials such as alumina foams [17] and metal foams [18].

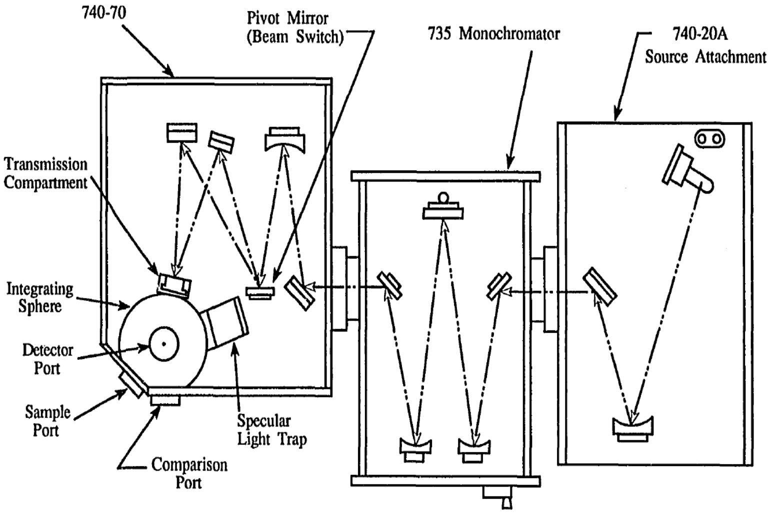

Figure 2.3: Schematic diagram of test apparatus to measure Transmissivity and reflectivity [4]

2.2 Unit Cell Approach

The unit cell approach is based on a simple assumption that a foam can be modeled as repetitive group of idealized unit cells of a certain shape. Hence, studying the local properties of that shape enables us to determine the global properties of the foam. Unit cell approach was utilized to all types of foam properties like pressure drop, volumetric heat transfer coefficient, thermal conductivity, and radiation properties. However, upto the knowledge of the author, it was never utilized to study all the properties at once.

One of the most important aspects in the unit cell approach is the selection of its shape. Therefore, this section starts by summarizing unit cell shapes used in the literature then presents the work done utilizing them.

2.2.1 Unit Cell Shapes

There are two extinct types of unit cells based on the way they are numerically constructed:

- **Volumetric based:** Where the unit cell volume is made of a solid material, then hollowed by certain volumes and shapes.
- **Struts based:** Where the edges of the unit cell are made of ligaments of a certain cross-section and thickness, and the rest of the unit cell volume is hollow.

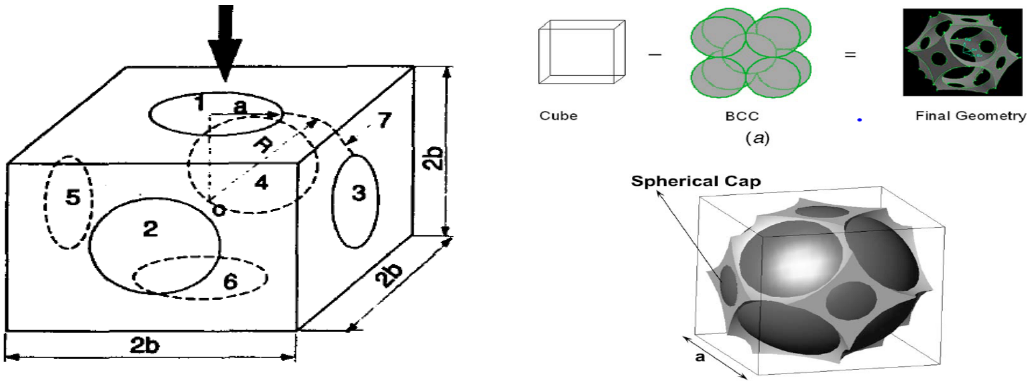

(a) Solid Cube Hollowed by a sphere in its Center [19]

(b) Solid Cube Hollowed by Body Centered Cell of Spheres [20].

Figure 2.4: Unit Cell Models Constructed by Volumetric Method.

In volumetric construction; the base shape considered is usually a solid cube which is then hollowed by a hollowing element,usually a sphere or set of spheres. Hollowing spheres number, position, and diameter all effect the final shape and some properties of the unit cell. To match the porosity of modeled foam the diameter of the hollowing spheres should be changed. To match the pore density in Pores Per Inch (PPI) of the modeled foam both the base cube and the hollowing

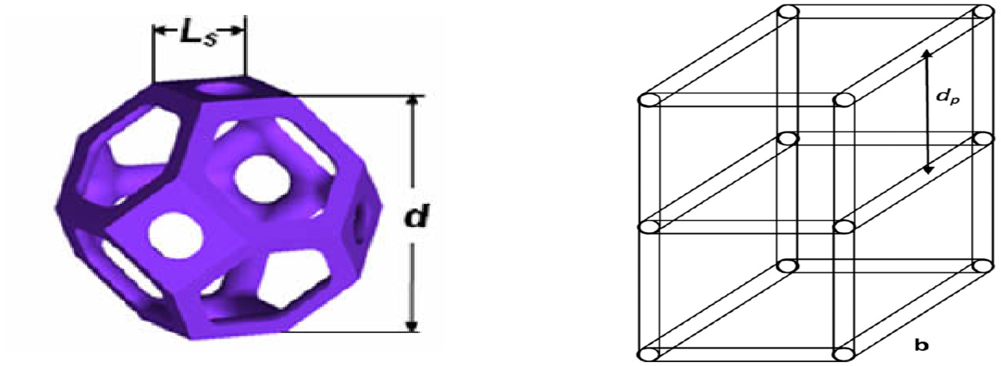

(a) Tetrakaidecahedron unit cell with clyndrical ligaments and round fillets [2].

(b) Cube simplified unit cell [21].

Figure 2.5: Unit Cell Models Constructed by Nodes and Ligaments Method.

spheres sizes should change. Attention has to be taken when selecting the hollowing spheres positions and diameters to assure that the unit cell has open cell construction and to eliminate any discontinuity in the solid phase. This method easy to construct, however, it has some drawbacks. One drawback is that the produced shape of the flakes is highly three dimensional and requires a large number of elements in order to accurately model it. That increases the complexity of the model and leads to longer and more intense computational time and power when modeling fluid flow and heat transfer within the unit cell. Additionally, the produced shape does not always produce a space filling tessellation, which is another disadvantage. Figure 2.4 shows two examples of volumetric base unit cell construction.

On the other hand, strut based construction is done by first selecting the location of the nodes in the three dimensional space. The position of the nodes are usually the vertices of a space filling terrestial. Then the ligament are built on the edges of the space filling terrestial to achieve the connection between the nodes. The selection of the space filling terrestial, the shape of the ligaments and the applied to the ligaments joints are the three factors that determines the properties of the unit cell. The nodes location can be also determined by image processing methods, or statistical methods. Ligaments cross-section can be in any shape; the most common shapes are circles, concaved triangular and convex triangular shapes with convex triangular cross-section ligaments giving the best results [20]. The advantage of this method is that it allows for control on the ligaments shape. It also easier to make sure that the produced unit cell produces a space filling terrestrial. Therefore this method is favored.

2.2.2 Pressure Drop and Volumetric Heat Transfer Coefficient

Since the determination of presssure drop and volumetric heat transfer coefficient characteristics of a foam is easily achieved by experimental methods, the use of unit cell approach in this area was limited. Additionally, fluid flow simulation requires more than one unit cell to achieve fully developed flow. Therefore, geometries constructed of multiples of repeating unit cells were used to obtain pressure drop and volumetric heat transfer coefficient characteristics of foams. Figure 2.6 shows construction of such setup. The results obtained from this method by Wu et.al. [2, 5] complies well with the results obtained by experimental method.

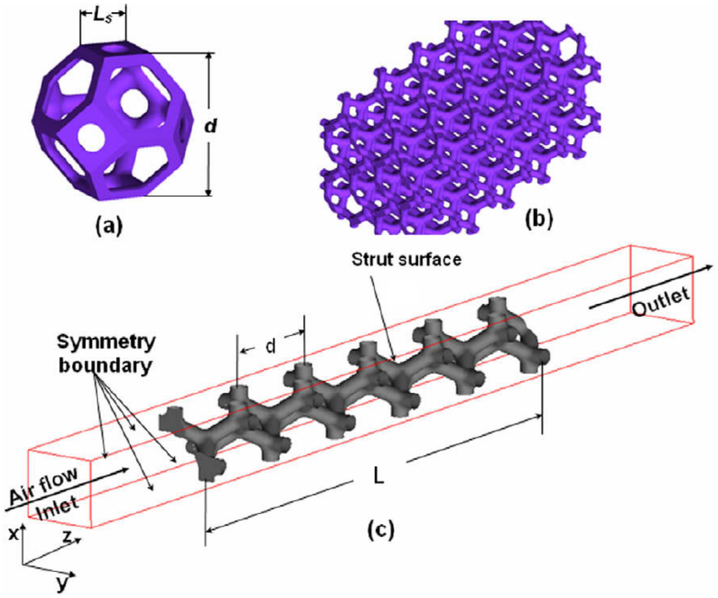

(a) Unit tetrakaidecahedron cell, (b) bulk foams formed by packed tetrakaidecahedrons and (c) computational domain and boundary conditions.

Figure 2.6: Geometry Used by Wu et al [2, 5] to determine Pressure Drop and Volumetric Heat Transfer Coefficient

2.2.3 Thermal Conductivity

Given the complexity of measuring the thermal conductivity experimentally, unit cell approach was widely used in the literature to obtain the thermal conductivity of ceramic foams. Based on the intended application of the foam in a given study; two temperature ranges were studied; high temperature range above 200°C where radiation plays the major role in the heat diffusion process and a low temperature range where radiation could be neglected [12]

1. Conduction only models.

   In 2009, Coquard and Baillis developed a numerical model to estimate the reliability existing models for finding the effective thermal conductivity in the absence of radiation [22] They found that the porosity has the largest effect in determining the effective thermal conductivity, and the shape of the struts and lumps had a secondary role.

More recent correlations were derived for metal foams by Yang et al [23] and Yao el al [24] However, these relations were derived for metallic foams and has not been proven to be accurate with ceramic foams.

However, since the intended application of the ceramic foam is in solar receivers, only models considering high temperature ranges with the presence of radiation should be considered.

2. Conduction + Radiation model

   A unit cell with BCC structure was used by J.E. Li et.al. to thoroughly evaluate the thermal conductivity of ceramic foams at high temperatures [25] The effect of both structural and optical properties were studied and validated against available published data. The conductive heat transfer was found analytically by applying model suggested by Boomsma and Poulikakos [23] which only depends on geometrical factors and solid phase thermal conductivity. Radiative heat transfer was also derived analytically making use of the Rosseland approximation and substituting the refractive value of ceramics by n. The equivalent thermal conductivity is then the superposition of both conductive and radiative conductivities.

$$Q_{rad} = -\lambda_{rad}\frac{dT}{dz} \tag{2.4}$$

with

$$\lambda_{rad} = \frac{16n\sigma T^3}{3\beta} \tag{2.5}$$

2.2.4 Radiation Properties

There are three radiation properties that can be determined from a unit cell model; the scattering coefficient, absorption coefficient, and the scattering phase function. For a bcc unit cell with isotropic solid phase reflectance, the radiation properties was found analytically by Li [25]. His derived results were found to be with good conformation with experimental results.

In 1997, X. Fu et al [19] developed a numerical model to measure the transmissivity and the reflectance of a unit cell consisting of a solid cube hollowed by a sphere Fig.2.4 . Reflectance and transmittance values were used to derive the effective radiative properties; the extinction coefficient and the scattering albedo. Simulations for different pore diameter and solid phase reflectance were done. Their findings were within 15% from experimental data.

2.2.5 Exact Modelling Approach

This method utilizes CT scans using x-rays to 3D scan a foam and then foam geometry is reconstructed using computer aided programs. However, this process is not straight forward and require expensive instruments and computer power. Therefore it was not widely used in the literature. In a recent studyby G.L. Vignoles and A. Ortona a model for measuring the effective thermal conductivity

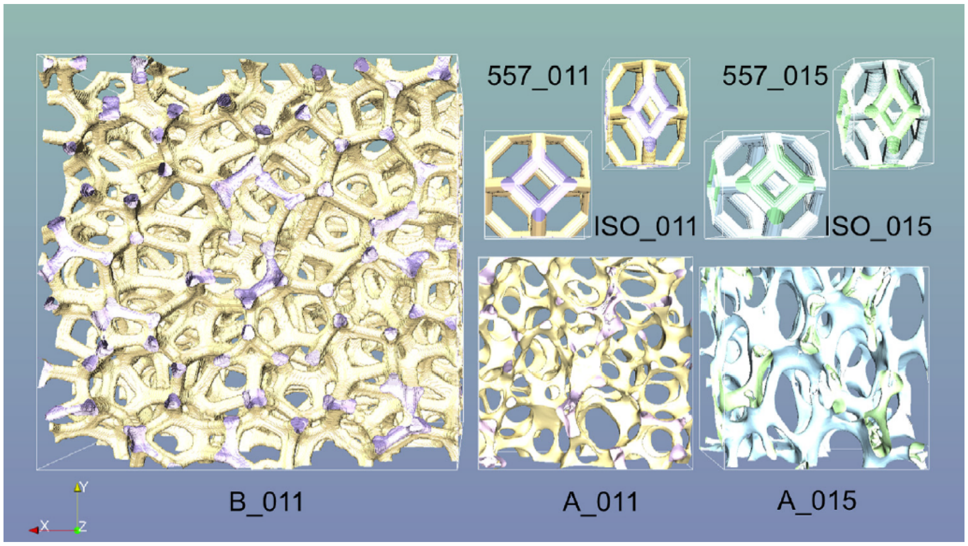

Figure 2.7: Scanned and modeled geometries as obtained from [6].

(conduction + radiation) of a foam using a real geometry and a unit cell shaped geometry was developed [6]. The results verified that simplified geometries used in literature give similar results to exact modeling with less time, cost, and computational power. Simplified geometries results were within ±10% of the exact model values. Another recent paper studied spectral emittance of silicon carbide foams using exact modeling technique [26] The study also found the size of smallest representative elementary volume to characterize the normal spectral emittance for different porosities and pore diameters. However, up to the knowledge of the author, exact modeling method has been used to model all modes of heat transfer at the same time.

2.3 Concluding Remarks on Literature Review

To summarize and conclude, the unit cell approach is a simplified model that can be used to model fluid flow and heat transfer in ceramic foams using limited time and computational resources. This method was successfully used in the literature and gave accurate results when matched to experimental data. However, the three modes of heat transfer were not modeled simultaneously using the unit cell method. Hence, there is a need to develop a setup utilizing the unit cell simplified approach to model all modes of heat transfer within this type of ceramic foams. This will provide better understanding of the fluid flow and heat transfer phenomena within ceramic foams which is essential to create general guidelines for designing a ceramic foam concentrated solar absorber.

CHAPTER 3

OBJECTIVES AND METHODOLOGY

This chapter presents the general and specific objectives of this work. Also, it describes the methodology used to achieve these objectives.

3.1 Objectives

The objective of this work is to model the three modes of heat transfer (conduction, convection, radiation) simultaneously in a unit cell model of ceramic foams used in concentrated solar absorbers in order to contribute some guidelines for designing the optimum concentrated solar absorber.

3.1.1 Specific Objectives

1. Identify the main parameters affecting the thermal performance of ceramic foam absorbers.
2. Develop a model that considers all modes of heat transfer (conduction, convection, radiation) inside the ceramic foam absorber.
3. Implement a systematic and simplified approach for analyzing the heat transfer inside the ceramic foam absorbers.
4. Suggest some design and operation guidelines for concentrated solar absorbers.

3.2 Methodology

A numerical approach utilizing the unit cell method is selected to tackle the problem. A commercial computational fluid dynamics (CFD) program is to be utilized to solve the fluid flow, energy and radiation equations. Various boundary and operation conditions are studied in order to understand their effect on the overall performance of the ceramic foam as solar absorbers. Some results are compared against published resources for validation.

3.2.1 Detailed Tasks

1. Identify the main parameters affecting the thermal performance of ceramic foam absorbers.

    (a) Conduct an updated literature review to identify all parameters affecting thermal performance of ceramic foam absorbers.
    (b) Conduct a comparative review to illustrate the importance of each parameter.
    (c) Select the 4-5 of the most important parameters to be studied.

2. Develop a model that considers all modes of heat transfer inside the ceramic foam absorber.
    (a) Formulate the problem of all modes of heat transfer in ceramic foams.
    (b) State assumptions and simplifications on the full mathematical model.
    (c) Develop a numerical model utilizing the simplifications and assumptions.

3. Implement a systematic and simplified approach for analyzing fluid flow and heat transfer inside the ceramic foam absorbers.
    (a) Run - Conduct numerical simulations for proposed scenarios under different design and operating parameters.
    (b) Analyze the numerical results and extract the main trends.
    (c) Validate the numerical models against published experimental or numerical data.

4. Suggest some design and operation guidelines for concentrated solar absorbers.

CHAPTER 4

PARAMETERS AFFECTING PERFORMANCE OF CERAMIC FOAMS

This chapter is an extension to the literature review with deep and detailed study of parameters affecting the performance of ceramic foams as volumetric solar recievers. It shows - in five tables - the effect of various studied parameters on other variables that effect the performance of foams as solar absorbers directly or indirectly. The calculated sensitivity is defined as the normalized change in the affected parameter over the normalized change in the studied parameter.

$$Sensitivity = \frac{\dfrac{Affected\,para.\,Max - Affected\,para.\,Min}{Affected\,para.\,Avrg}}{\dfrac{Studied\,para.\,Max - Studied\,para.\,Min}{Studied\,para.\,Avrg}} \tag{4.1}$$

Tables 4.1 through 4.5 shows the effects of material properties, porosity, pore size and other design parameters, characteristics of heated flow, and solar irradiation on various parameters affecting the performance of ceramic foams as solar absorbers.

Table 4.1 shows that the thermal conductivity of the solid foam material and its surface reflectivity are the two major material properties affecting the performance of ceramic foams. The foam's solid material thermal conductivity mainly affects the effective thermal conductivity, temperature distribution in the foam, and the overall efficiency of the foam by small amount. While the surface reflectivity affects the effective radiative properties such as the effective reflectance, transmittance and extinction coefficient. Hence, affecting the radiative conductivity. Therefore, thermal conductivity of the foam solid material and its surface reflectivity are considered as variable parameters in this study.

Tables 4.2 and 4.2 show the great effect of porosity, pore size and other design parameters on the performance parameters of ceramic foams. The effects these design parameters extend to a wide range of performance parameters such as effective radiative properties of foam, fluid flow and heat transfer performance, overall efficiency of the foam, and the air outlet temperature. Therefore, foam porosity and pore size are identified as main design parameters that affect the performance of ceramic foam absorbers. However, since studying these parameter will require a separate geometry and mesh for each case, it was not considered as a variable parameter in this study.

Finally, Tables 4.4 and 4.5 show the effect of operating conditions such as the fluid type, flowrate, or solar irradiation on various fluid flow, heat transfer and overall performance of ceramic foams. Fluid flowrate of fluid and the Reynold's number are both controlled by changing the mass flax of the fluid. Therefore it is considered as study parameter. The magnitude of the irradiation is the other operation condition considered in this study.

The conclusion made from this chapter can be summarized as follows:

- The performance of ceramic foams is affected by two types of parateres; design parameters and operation parameters.
- The design parameters can be further divided into two types; solid material properties and foam characteristics and treatment.
- The most important solid material properties are the thermal conductivity and the surface reflectivity.
- The most critical foam characteristics and treatment are the porosity and the pore size ie; pore density.
- The most critical operating conditions are the fluid mass flowrate and the magnitude of the solar irradiation.

Hence, the four parameters chosen to be studied in this thesis are: the solid material thermal conductivity and its surface reflectivity, the mass flowrate of fluid and the magnitude of irradiation.

Table 4.1: Effect of Material Properties

Type		**Studied parameter**	**Range**			**Affected Parameter**	**Values**		**Sensitivity**	**References**
			Min	**Max**			**Min**	**Max**		
Design	**Material**	Thermal Conductivity	0.16	13.4		Eff. thermal conductivity	0.06	2.80	0.98	[22]
			1	10		Temperature distribution	1,500	3,050	0.42	[27]
						Stability of temp. field				[27]
			1	100		Effeciency	0.66	0.75	0.07	[28]
		Max. Operation Temp.				Effeciency				[29]
		Extinction Coeff.				Temp. Profiles				[30]
		Composition				Change over exposure				[31]
		Surface Reflectivity	0.1	0.99		Eff. Reflectance	0.01	0.42	1.17	[19]
			0.1	0.99		Eff. Transmittance	0.04	0.44	1.02	[19]
			0.1	0.99		Extinction Coeff.	1,100	500	0.46	[19]
			0.1	0.99		Scattering Albedo	0.02	0.99	1.18	[19]
			0.1	0.99		Radiative conductivity				[32]

Table 4.2: Effect of Porosity

Type		**Studied parameter**	**Range**			**Affected Parameter**	**Values**		**Sensitivity**	**References**
			Min	**Max**			**Min**	**Max**		
Design	**Treatment**	Porosity	0.55	0.95		Eff. Reflectance	0.05	0.40	2.92	[19]
			0.55	0.95		Eff. Transmittance	0.05	0.56	3.14	[19]
			0.6	0.95		Extinction Coeff.	1,100	400	2.07	[19]
			0.6	0.95		Scattering Albedo	0.02	0.65	4.16	[19]
			0.7	0.99		Eff. Thermal Conductivity	2.80	0.10	5.43	[20],[33], [34], [22], [32]
			0.91	0.98		Eff. Thermal Conductivity	10	1	22	
			0.94	0.98		Permeability	0.01	0.02	9.31	[20]
			0.55	0.85		Pressure drop	8.00	2.00	2.80	[2]
			0.66	0.85		Inertial Coeff.	5.00E-4	2.40E-3	5.21	[2]
			0.66	0.85		Permiability Coeff.	1.90E-8	4.20E-8	3.00	[2]
			0.7	0.94		Heat transfer Coeff.	310	360	0.51	[5]
			0.74	0.92		Effeciency	0.73	0.76	0.22	[28],[29, 35]
			0.74	0.92		Foam Front Tem	1,242	1,210	0.12	[28]
						Air outlet Temp				[29, 35]

Table 4.3: Effect of Pore Size and Other Complications

Type		**Studied parameter**	**Range**			**Affected Parameter**	**Values**		**Sensitivity**	**References**
			Min	**Max**			**Min**	**Max**		
Design	**Treatment**	Pore Size	4	26		Extinction Coeff.	3,500	500	1.02	[19],[36]
						Nusselt Number				[20]
						Radiative conductivity				[33], [32]
			1.55	4.49		Pressure drop	1.00E+5	2.50E+4	1.23	[2]
			0.7	2.8		Inertial coefficient	0.00	0.00	1.05	[2]
			0.7	2.8		Permiability Coeff.	0.00	0.00	1.44	[2]
			10	45		Volumetric Heat transfer Coeff.	6.50E+4	2.40E+5	0.90	[29, 35]
			1.41	2.83		Local Heat transfer Coeff.	360	225	0.69	[5], [29, 35]
		Pores & ligaments Shape				Radiative conductivity				[33]
			1	2		Eff. thermal conductivity	0.80	2.80	1.67	[22], [23]
						Extinction Coeff.				[36]
Design	**Others**	2 - 3 mm holes in porous structure				Pressure Drop	4.00E+4	1.80E+5		[2]
		2 layes different PPI	1	2		Pressure Drop				[29, 35]
			1	2		Efficiency	75	92	0.31	[29, 35]
			1	2		Air Outlet Temp	550	850	0.64	[29, 35]

Table 4.4: Effect of Operation Conditions and Flowrate

Type		**Studied parameter**	**Range**			**Affected Parameter**	**Values**		**Sensitivity**	**References**
			Min	**Max**			**Min**	**Max**		
Operating Conditions	**Foam**	Solid phase Temperature				Radiative Conductivity				[33],[21], [36],[32], [32]
	Flow	Fluid				Fluid max Temp	1,750	1,993	0.19	[37]
						Re-Radiation losses	0.08	0.42	2.01	[37]
						Efficiency	0.65	0.80	0.31	
						Absorbed power	0.55	0.89	0.69	[37]
		Reynold's Number	0.1	10		Friction factor	0.10	10.00	1.00	[20]
			3	5		Pressure drop	3.70E+4	9.00E+4	1.67	[2]
			129	388		Local heat transfer coeffiient	850	1,200	0.34	[5]
			129	388		Local Nusselt Number	18	25	0.32	[5]
			1	200		Volumetric Heat transfer Coeff.	1	30	0.94	
			5	12		Volumetric Heat transfer Coeff.	1.65E+5	2.25E+5	0.37	[29]
			0.5	4.5		Volumetric Heat transfer Coeff.	1.50E+5	3.80E+5	0.54	[5]
		Flowrate	2.25	3.5		Efficiency	0.45	0.80	1.29	[37], [28]
			0.45	0.65		Efficiency	0.67	0.78	0.42	
			2.4	3		Output air Temp	1,983	1,903	0.19	[37], [28]
			0.45	0.65		Output air Temp	1,130	975	0.40	
			3.9	6		Fluid max Temp	1,878	1,343	0.78	[37]
			2.67	3.44		Re-Radiation losses	0.42	0.26	1.82	[37]
			2.67	3.44		Absorbed power	0.55	0.70	0.93	[37]

Table 4.5: Effect of Solar Irradiation

Type		**Studied parameter**	**Range**			**Affected Parameter**	**Values**		**Sensitivity**	**References**
			Min	**Max**			**Min**	**Max**		
Operating Conditions	**Solar Radiation**	Intensity	400	800		Solid Temp Profile	900	1,300	0.55	[28]
			400	800		Fluid Temp Profile	850	1,200	0.51	[28]
		Intensity Mass flowrate	300	750		Efficiency	90	75	0.21	[29, 35]
			300	750		Air Outlet Temp 2 layers	300	550	0.69	[29, 35]
		Profile				Efficiency				[38]
						Maximum Temp				[38]

CHAPTER 5

NUMERICAL AND MATHEMATICAL MODELING

This chapter starts by describing the unit cell geometry and construction. The flow field, simulation domain and boundary conditions are then described. Followed by overview on the numerical mesh used. The basic assumptions made to simplify the complex nature of the problem is presented. Finally, the mathematical formulas used in the numerical modeling and its post-processing is shown.

5.1 Geometry

From the literature review section 2.2.1, it has been identified that a truncated octahedron strut consisting of circular beams -ligaments- unit cell gives the closest results to experimental studies in fluid flow and volumetric heat transfer coefficient [2, 5]. Therefore, this method is used to generate the basic unit cell shape. The octahedron edge length is set to $1mm$. The ligaments radius is set to $0.2mm$. This combinations produces a unit cell with a midsphere radius of $1.5mm$ which is the hydraulic diameter D of the unit cell. The unit cell is placed in the middle of a $2.83mm$ cube to make it more convinient when building multiple unit cell models. Therefore, square faces of the octahedron have only half cylindrical ligaments. The unit cell represents a foam of 89% porosity, and pore density of 12.7 pores per inch PPI. Figure 5.1(a , b) shows the unit cell geometry. The cell The geometrical properties of the unit cell approximately matches the geometrical properties of an available ceramic foam intended for future use in a concentrated solar absorber.

Two multiple unit cells models are constructed using the basic unit cell. Both geometries are two unit cells high and wide. However, the first multiple cells model is two cells long -in the flow and irradiation direction- and the second multiple cells model is three cells long. The multiple unit cells models are abbreviated as 2^3 & $2^2 \times 3$ respectively. In both geometries, a central unit or two unit cells are place in the middle of the assembly then surrounded by half a unit cell from every direction. The multiple unit cells geometries are tilted by $22.5°$ around the Y and Z directions in order to prevent the front ligaments from shading the ligaments in the back. This was done to improve the optical similarity between the real foam and the models.

The geometrical models are placed in the middle of a flow domain which has same height and width of the models. The length of the domain is the model length plus two unit cells length, with an inlet and an outlet placed $2.83mm$ in front and at the back of the model.

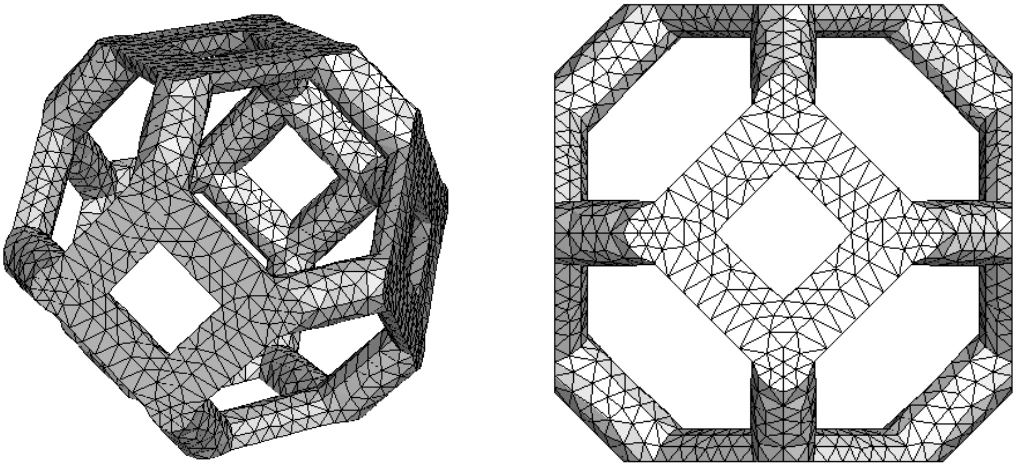

(a) Isometric view (b) Front view

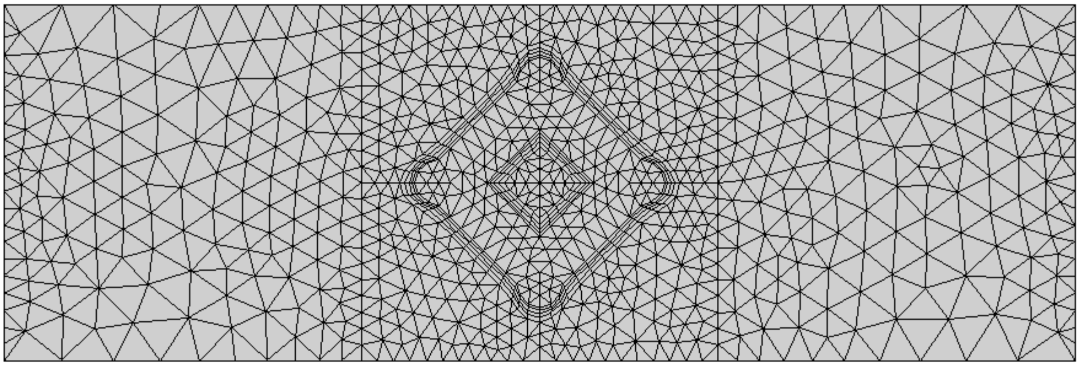

(c) Domain mesh - Side view

Figure 5.1: Single unit cell model

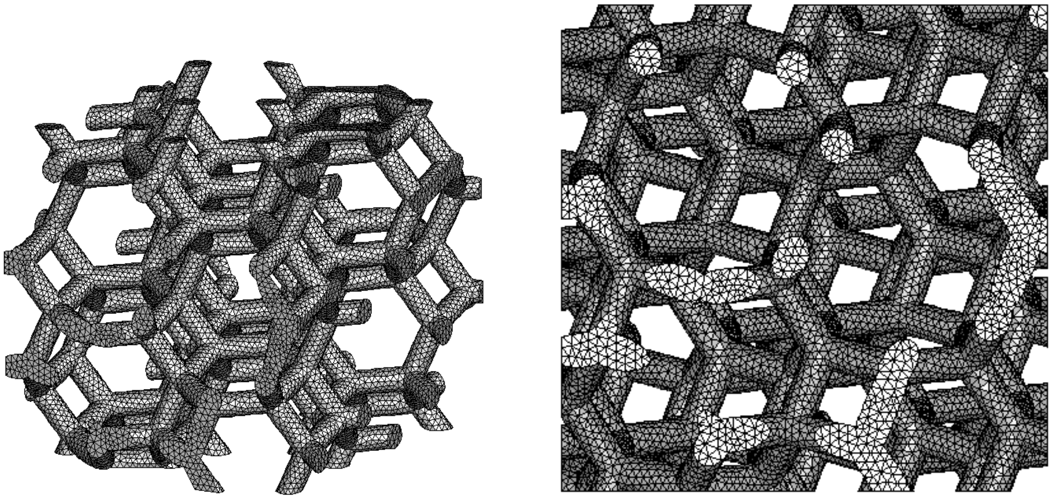

(a) Isometric view (b) Front view

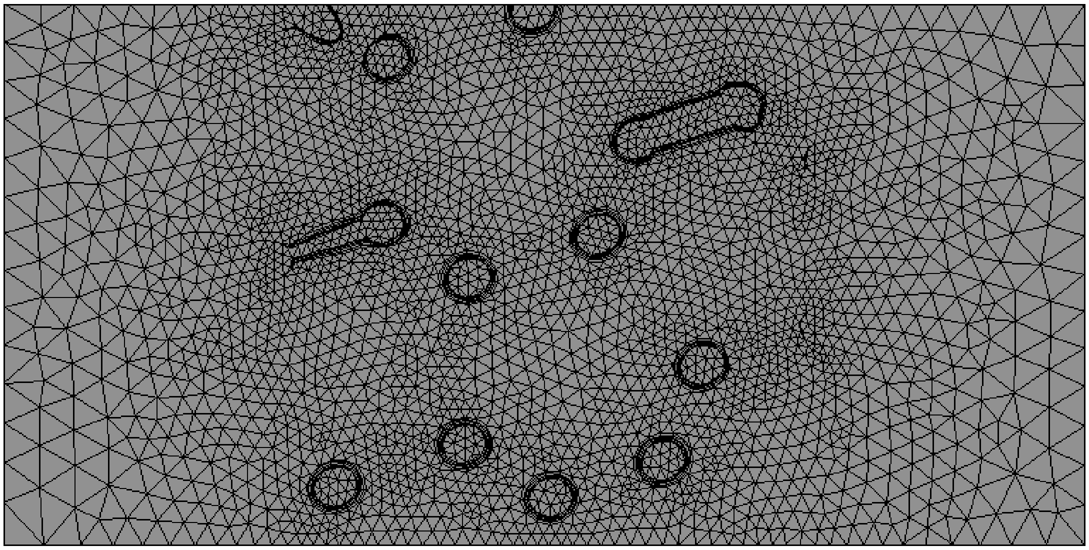

(c) Domain mesh - Side view

Figure 5.2: 2^3 Multiple unit cells model

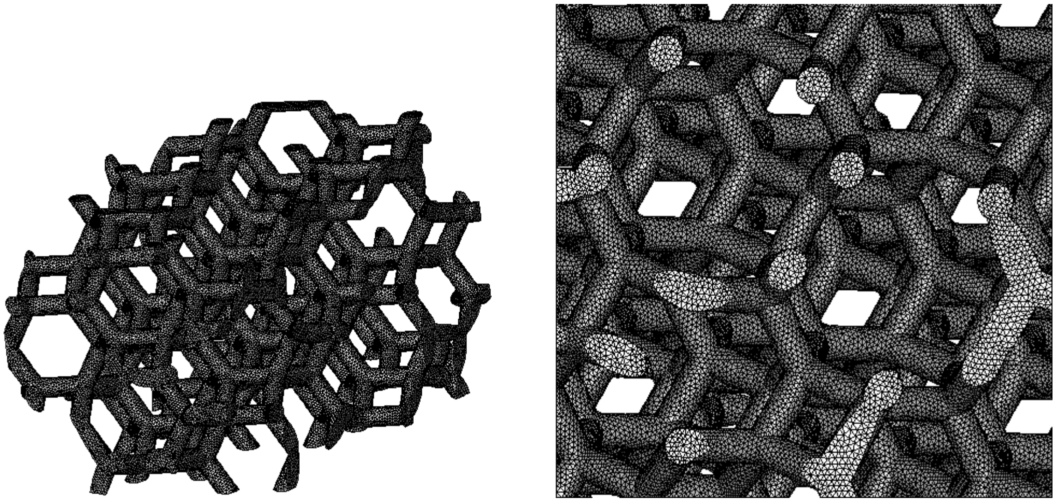

(a) Isometric view

(b) Front view

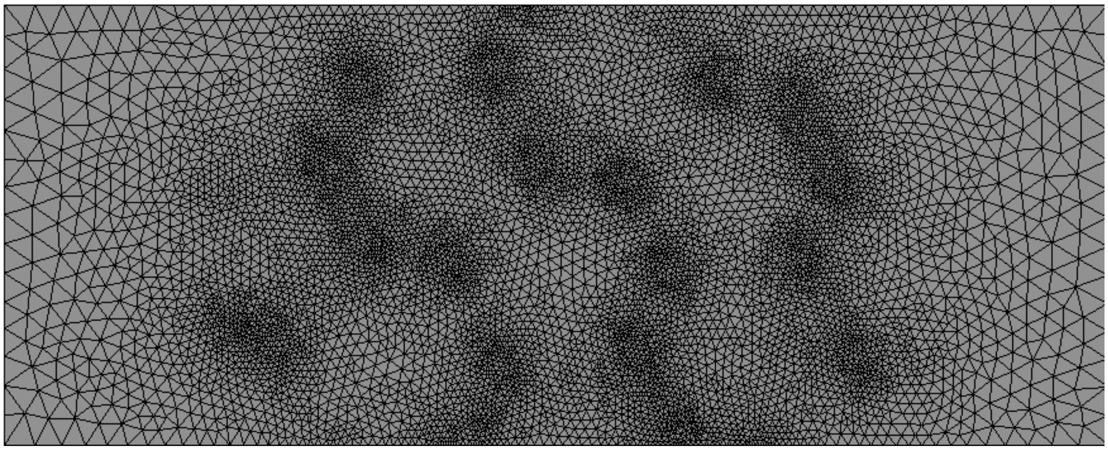

(c) Domain mesh - Side view

Figure 5.3: $2^2 \times 3$ Multiple unit cells model

5.2 Mesh

The geometry and the fluid domain is meshed using tetrahedral cells to accurately capture the details of the geometry. A finer mesh is added to the fluid domain near the ligaments in order to capture the boundary layer and the heat transfer. A mesh independency study was done on the single cell model and similar mesh setting was used for all models.

5.3 Assumptions

- **Steady State:** The problem is assumed to be a steady state problem since non of the boundary conditions is changing over time. Therefore, all partial derivatives with respect to time are set to zero $\partial/\partial t = 0$. This is an acceptable approximation since the solar irradiation does not change rapidly through the day, unless a cloud passes and blocks the sun. Also the thermal capacitance of the absorber is not large. Therefore, the system does not take a lot of time to reach steady state if any of the parameters changes.

- **Turbulent Flow:** The flow behavior is assumed to be turbulent since the Reynold's number $Re > 200$ and the widely accepted theory that turbulent flow in porous medium starts from $Re = 100$ [39]. The tubulence model used is the RNG $k - \epsilon$ model.

- **No radiation side scattering:** This assumption is imposed due to the use of symmetry boundary condition on all sides of the unit cell. It can be visualized as if the radiation beams does not get scattered to the sides. Since we assume that the unit cell is part of a foam, any scattered radiation from the unit cell to the sides is replaced by a similar scattered beam from neighboring cells to the cell of interest. Therefore, the net side scattering will be zero and the assumption is justified.

- **No Temperature jump:** This means that the temperature of the fluid adjacent to the solids have the same temperature.

Air Properties

- **Non Participating:** The air is assumed to be a non participating medium ie; it does not absorb, scatter or emit solar radiation.
- **Variable Density:** Since the temperature change within the domain is greater than $50K$; air density is assumed to follow the ideal gas law.
- **Piece-wise Linear Properties:** Air thermal conductivity, viscosity and thermal capacity are assumed to be piece wise linear with properties values input every $300K$ from $300K$ to $1500K$ at atmospheric pressure.

Solid Material Properties

- **Temperature Independent Properties:** All solid material properties including thermal conductivity, thermal capacity and surface emmisivity are assumed to be constant and does not change with temperature.

- **Diffused Surface:** Emissivity and absorbtivity do not depend on direction. Therefore emitted intensity is uniform over all directions.

- **Gray Surface:** Emissivity and absorbtivity do not depend on beam wavelength.

5.4 Model Equations & Boundary Conditions

The main equations governing the solution of the problem are the fluid continuity, momentum and energy equations. These equations are obtained from Fluent theory guide and simplified to properly represent the studied problem [9]. The steady state continuity with no source terms is given as:

$$\nabla \cdot \big(\rho \vec{v}\big) = 0 \tag{5.1}$$

where ρ is the fluid density and $\vec{v}$ is the velocity vector.

The steady state conservation of momentum without gravitational or external body forces equation is given by:

$$\nabla \cdot \big(\rho \vec{v}\vec{v}\big) = -\nabla p + \nabla \cdot \big(\overline{\overline{\tau}}\big) \tag{5.2}$$

where p is the static pressure, $\overline{\overline{\tau}}$ is the stress tensor given by:

$$\overline{\overline{\tau}} = \mu\Big[\big(\nabla \vec{v} + \nabla \vec{v}^{T}\big) - \frac{2}{3}\nabla \cdot \vec{v} I\Big] \tag{5.3}$$

where μ is the molecular viscosity, I is the unit tensor, and the density of the air assuming ideal gas law is given by:

$$\rho = \frac{p_{op} + p}{\frac{R}{M_w} T} \tag{5.4}$$

where p_{op} is operating pressure, R is universal gas constant, and M_w is the molecular weight. The temperature T will be computed from the energy equation which is given by:

$$\nabla \cdot \big(\vec{v}(\rho E + p)\big) = \nabla \cdot \left(k \nabla T - \sum_j h_j \vec{J_j} + \big(\overline{\overline{\tau}}_{eff} \cdot \vec{v}\big)\right) + S_h \tag{5.5}$$

Where $\vec{J_j}$ is the diffusion flux of species j, S_h includes the volumetric heat sources, and E described by :

$$E = h - \frac{p}{\rho} + \frac{v^2}{2} \tag{5.6}$$

where sensible enthalpy h is defined as:

$$h = \int\limits_{T_{ref}}^{T} c_p dT \tag{5.7}$$

The energy equation can be simplified in solid regions to:

$$0 = \nabla \cdot \big(k \nabla T\big) + S_h \tag{5.8}$$

The surface to surface radiation model equation can be expressed as:

$$q_{out,k} = \epsilon_k \sigma {T_k}^4 + \rho_k \sum_{j=1}^{N} F_{jk}\, q_{out,j} \tag{5.9}$$

where $q_{out,k}$ is the energy flux leaving the surface k andϵ_k is the emissivity of the surface. $\sigma$is the Stefan-Boltzmann constant. $q_{out,j}$ is the energy flux leaving the surface j. T_k is the temperature of surface k, ρ_k is its reflectivity. F_{kj} is the view factor between surface k and surface j which can be calculated from:

$$F_{kj} = \frac{1}{A_k} \int_{A_k} \int_{A_j} \frac{\theta_k cos\theta_j}{\pi r^2}\, \delta_{kj} dA_k dA_j \tag{5.10}$$

Where $A_j \& A_k$ are the areas of surfaces $j \& k$ respectively. $\theta_j \& \theta_k$ are the angles between the surfaces normal vectors and line r drawn between surfaces centroids. The whole radiation is equation is then added to the solid surface energy equation as source terms S_h

5.4.1 Boundary Conditions

For the given problem, boundary conditions are specified at the inlet, outlet, sides, and solid-fluid interface.

Inlet Boundary Conditions

The face of the simulation domain is set as a mass inlet with mass flowrate $\dot{m}$ as a study parameter. The inlet flow temperature T_{in} is set to 300 K. The flow direction is the positive X direction. Turbulence model is used with the turbulence intensity at the inlet is set to 5% and the turbulent viscosity ratio is set to 10. Thermal boundary conditions are set as

Solar ray tracing model parameters were set as following:

- **Sun Direction Vector:** $X = -1\, Y = 0\, Z = 0$
- **Direct Beam Intensity:** is set as a modeling parameter.
- **Diffuse Beam Intensity:** is set to zero.
- **Spectral Fraction:** is set to one.

Therefore, the incoming solar irradiation is inline with the flow direction, and the radiation beams are straight and parallel which is very close to the case of radiation on ceramic foam absorbers when the reflector dish is large and have a large curvature.

Sides Boundary Conditions

All boundary conditions at the sides of the simulation domain are set to symmetry. That forces the normal velocity and all normal gradients of all variables are set to zero at the symmetry planes. Therefore, there will be no convective and no diffusion fluxes through the sides and no heat transfer. Hence, all incoming energy from the inlet will be exiting through the outlet in different forms.

Outlet Boundary Conditions

The outlet is set to a pressure outlet with pressure at the outlet is set to atmospheric pressure. The far field temperature used for radiation calculations is set to be the same as the air exit temperature.

5.5 Performance Parameters Calculation

The results of the numerical simulation is reported in various parameters. Each of which is accordingly defined and calculated.The cell overall performance efficiency η is defined as the ratio of energy transferred to the fluid to the the total incident radiation on the cell.

$$\eta = \frac{\dot{H}_{out} - \dot{H}_{in}}{G * A_{cs}} \tag{5.11}$$

where $\dot{H}_{out}$ & $\dot{H}_{in}$ is the enthalpy flowrate in J/s in and out of the model respectively. G is the solar irradiation in $Watts$ and A_{cs} is the cross-sectional area of the unit cell in m^2.

The total pressure drop cross the unit cell ΔP is calculated by:

$$\Delta P = P_{out} - P_{in} \tag{5.12}$$

However, the pressure drop is reported as $-\Delta P/\Delta x$, where Δx is the geometrical model length.

Volumetric heat transfer coefficient h_v is defined as:

$$h_v = \frac{\dot{H}_{out} - \dot{H}_{in}}{\forall_c \left(\overline{T_s} - \overline{T_g}\right)} \tag{5.13}$$

h_v is calculated in $W/m^3 \cdot K$ where $\forall_c$ is the volume of the geometrical model in m^3, $\overline{T_s}$ is the average temperature of the ligaments and $\overline{T_g}$ is the average temperature of air in the model.

The Reynolds number Re is defined based on the superficial velocity at the inlet v_{in} by

$$Re = \frac{\rho \, v_{in} \, D}{\mu_{in}} \tag{5.14}$$

where D is the innersphere diameter of the unit cell and μ_{in} is the dynamic viscosity of air at the inlet.

The Nusselt Number Nu is calculated by:

$$Nu = \frac{h_v D^2}{k_g} \tag{5.15}$$

where k_g is the thermal conductivity of air.

A strong relation between the ratio of solar irradiation G in W/m^2 to the mass flux m'' in $kg/m^2 \cdot s$ and many performance parameters are observed. Therefore, this ratio is defined as the specific energy E_{SP} with unit of J/kg

$$E_{SP} = \frac{G}{m''} \tag{5.16}$$

CHAPTER 6

RESULTS

This chapter shows the results and findings of the thesis and presents it in two steps. First, a basic case of a given material properties and operating conditions is studied in detail for a single cell and multiple cells models. Second, a parametric study to understand the effect of different material properties and operating conditions on the performance of foam model is presented.

Table 6.1: Nomenclature

Symbol	**Meaning**	**Units**
D	Hydraulic Diameter	m
E_{SP}	Specific Energy	J/kg
G	Solar Irradiation	W/m^2
$\dot{H}$	Enthalpy Flowrate	J/s
Nu	Nusselt Number	
P	Static Pressure	Pa
Re	Reynold's Number	
T	Temperature	Kelvin
h_v	Volumetric Heat Transfer Coefficient	$W/m^3 \cdot K$
k	Thermal Conductivity	$W/m \cdot K$
m''	Mass Flux	$kg/m^2 \cdot s$
v	Velocity	m/s

Subscript	**Meaning**	
in	Inlet	
out	Outlet	
$AVRG$	Parametric Study Average	
MIN	Parametric Study Minimum	
MAX	Parametric Study Maximum	
$avrg$	Case Domain Average	
min	Case Domain Minimum	
max	Case Domain Maximum	
s	Solid	
g	Gas	

6.1 Basic Case

In this first section of the results a detailed discussion of the flow field and heat transfer within a single unit cell and assembly of 2^3 and $2^2 \times 3$ unit cells is sequentially presented. The basic case material properties and operation conditions are: $m'' = 12.5 kg/m^2 \cdot s$, $G = 2MW/m^2$, $k_s = 100W/m \cdot K$, $\epsilon_s = 0.9$.

Table 6.2: Basic Case Conditions

	Parameter	Value	Units
1	Solar Irradiation G	2	MW/m^2
2	Mass Flux m''	12.5	$kg/m^2 \cdot s$
3	Specific Energy E_{SP}	160	kJ/kg
4	Superficial Velocity v_{in}	10.2	m/s
5	Reynold's Number Re	$2,072$	
6	Surface Absorbtivity α_s	0.9	
7	Thermal Conductivity k_s	100	$W/m \cdot K$

6.1.1 Radiation Performance

Since the only thermal load on the system is the solar irradiation, it is logical to start the analysis by the studying the performance of the unit cell from a radiation point of view. A key parameter in determining the performance of an absorber is to evaluate how much it reflects, absorbs or transmits an incoming irradiation.

Figure 6.1 shows the absorbed and transmitted radiation as a percentage of the irradiation. The figure shows that 45% of the solar irradiation is transmitted through the single unit cell model. This can be explained by knowing that the

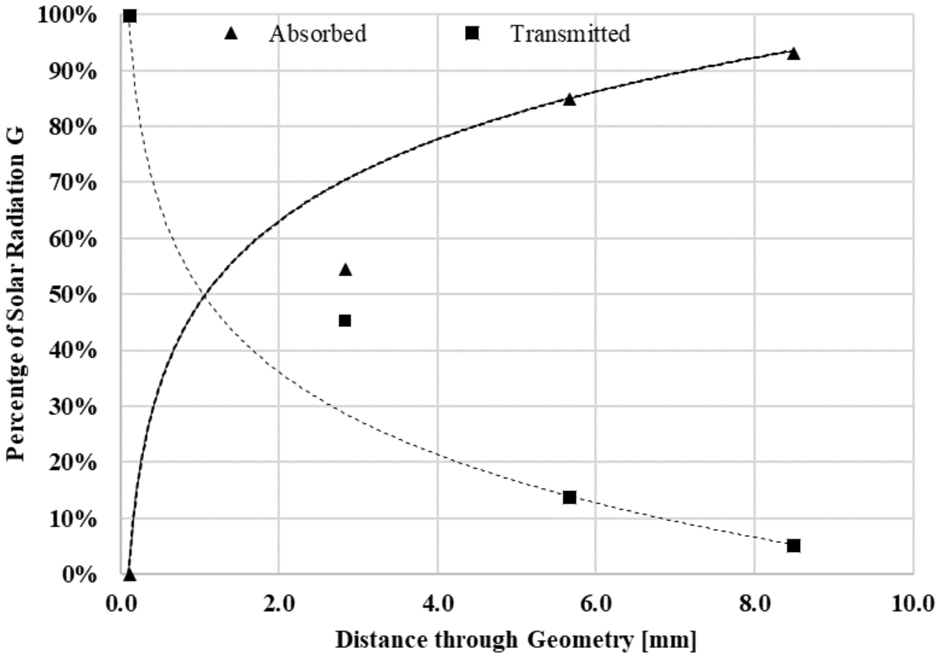

Figure 6.1: Basic case absorbed and transmitted percentage of irradiation.

projection area of the solid ligaments on the inlet area represents 57% of the total frontal area. Therefore, at least 43% of the solar radiation passes the unit cell directly without being interfered by any solids. The extra 2% in the transmitted portion of the radiation is due to the rays that passed the domain by multiple reflections from the ligaments. However, this value is overestimated since the back ligaments are shadowed due to the alignment and orientation of the single cell model. Figure 6.2 clearly shows this shadowing effect. In a more realistic model, the back ligaments are not fully shadowed and some of the radiation will be absorbed them. Therefore increasing the absorbed percentage of irradiation in single cell model and decreasing the transmitted percentage.

The normally reflected percentage of the radiation is only 1 % in all three geometries. This value is smaller than the expected value because the ligament surfaces are assumed to be diffused reflective surfaces and they reflect the incoming radiation in all directions in the same intensity. Therefore. most of the reflected radiation is reflected to the side and not in the normal direction. In addition, reflected radiation from the back ligaments is partially blocked from escaping the internal geometry by the front ligaments. Therefore, we conclude that the normally reflected radiation is mainly due to the first unit cell, and the contribution of the unit cell at the back can be neglected.

Although the current model does not calculate the scattered radiation on the sides of the computational domain, it is still able to capture the forward and backward scattered portion of the radiation beam which were shown to have the greatest portion of scattering effect [4].

Figure 6.2 shows the solar flux contours on the models. The solar flux values represent the net radiation flux on the surface. Therefore the maximum solar flux observed is equal to $1,800,000 W/m^2$ which is equal to:

$$I_{abs} = \alpha_s \times G \times cos\phi = 0.9 \times 2,000,000 \times 1 = 1,800,000 \, W/m^2$$

Also, The font ligament which are at an angle of $45° Degrees$ with the positive x-axis have maximum solar flux intensity of around $1,300,000 W/m^2$ which is equal to:

$$I_{abs} = \alpha_s \times G \times cos\phi = 0.9 \times 2,000,000 \times \frac{\sqrt{2}}{2} = 1,272,792 \, W/m^2$$

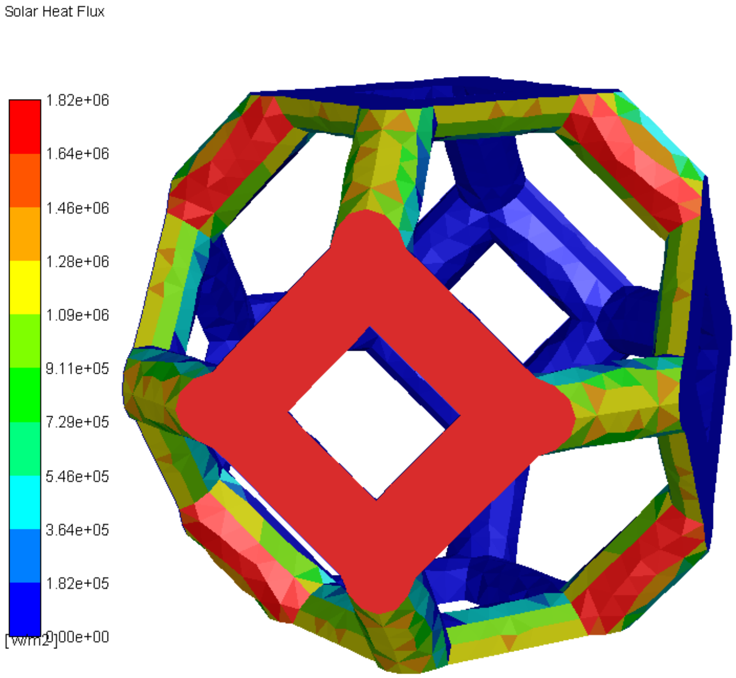

Figure 6.2: Solar flux contours on unit cell

6.1.2 Temperature Profiles

The temperature profiles shown in Fig. 6.3 are strongly related to the radiation flux profiles since the absorbed radiation is the only source of energy that heats the ligaments. However, temperature profiles does not follow the absorbed radiation profiles exactly. This is due to conduction within the ligaments which tend to diffuse the heat through the solid. This is the reason why we observe higher temperatures in the tilted ligaments than the normal facing ligaments further in the back which has higher radiation intensity. In this basic case the solid maximum temperature $T_{s,max}$ is $877\,K$ and the minimum temperature $T_{s,min}$ is $723\,K$ while the average solid temperature $\overline{T}_s$ is $801\,K$.

Figure 6.4 shows the temperature gradients within the solid ligaments in $Kelvin/m$. This quantity is of interest because the it introduces thermal stresses

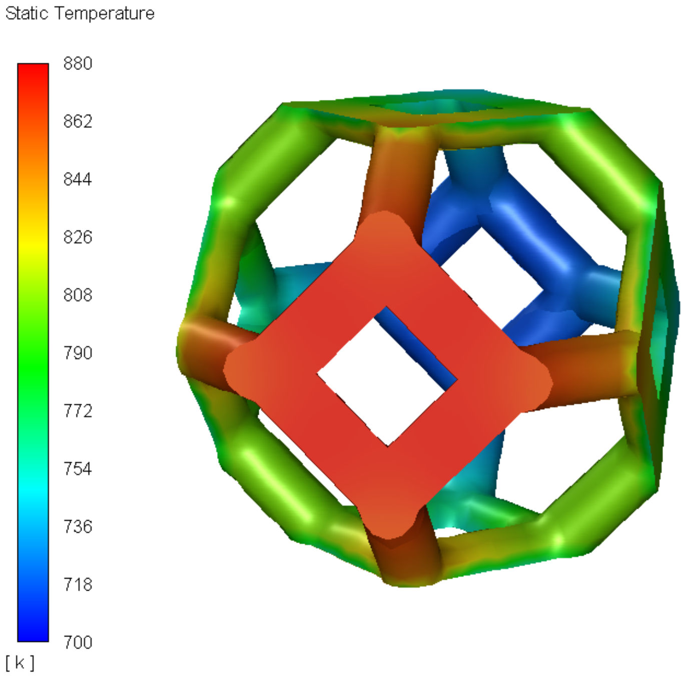

Figure 6.3: Temperature profiles on unit cell

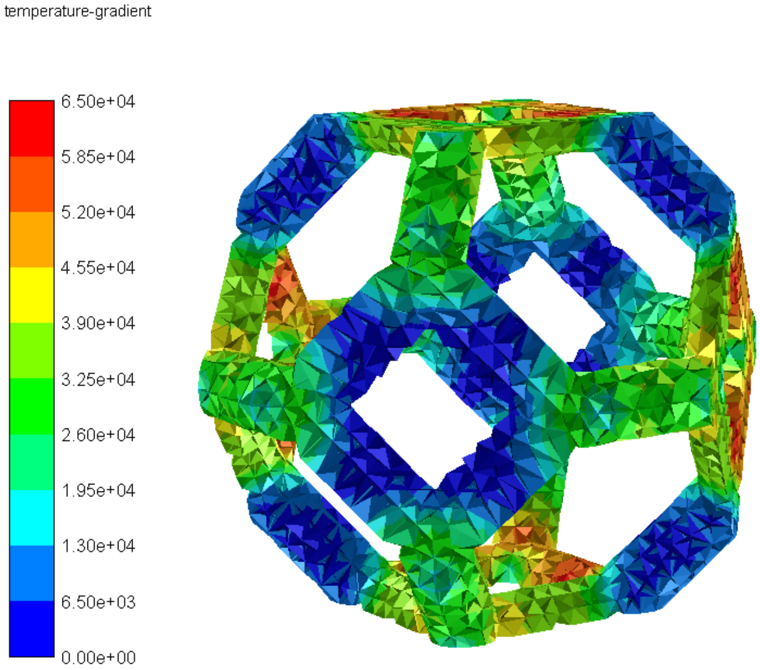

Figure 6.4: Temperature gradients on unit cell

in the ligaments. During the operation of such materials in concentrated solar absorbers, the material goes under cyclic thermal loads. The increase in the temperature gradients might cause thermal fatigue. A recent study by Ghazi has shown the effect of thermal cyclic loading on the mechanical integrity of the absorber material [1]. Thermal stresses were identified as the main cause of failure of alumina samples. Hence, this point is brought into attention. It is also clearly noticed that the front ligaments are blocking the irradiation from reaching the back ligaments directly.

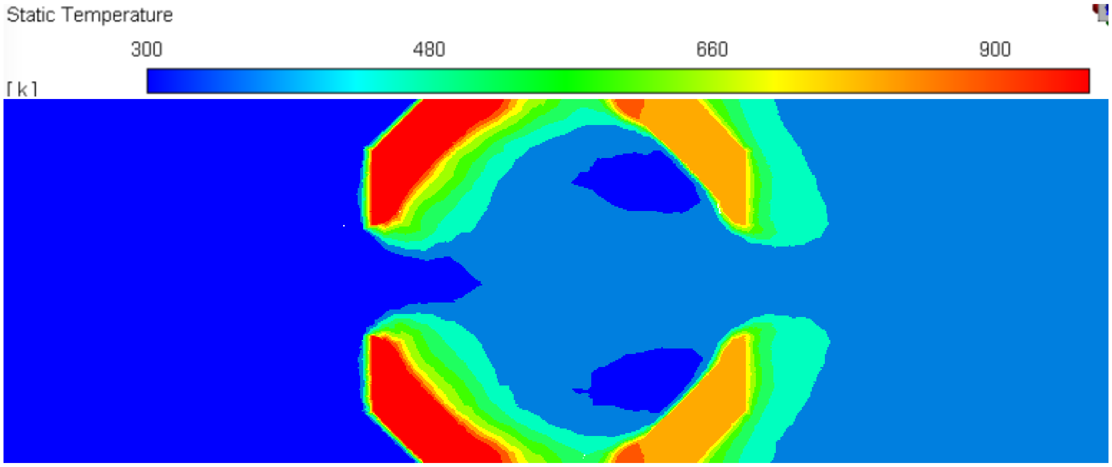

(a)Temperature profile on center plane

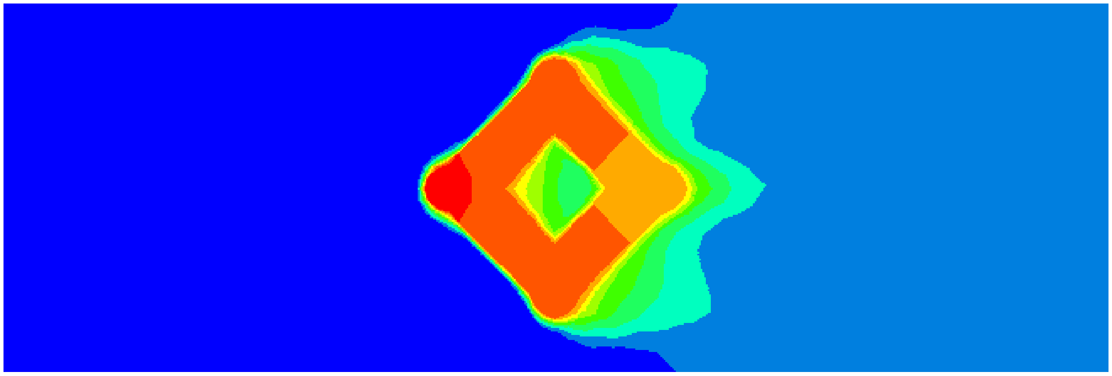

(b)Temperature profile on symmetry plane

Figure 6.5: Air temperature contours

Figure 6.5 shows the temperature contours of the fluid field. The average air temperature at the outlet is $386\,K$. Two important observations; firstly, the maximum temperature of air happens in the side symmetry plane just behind the first ligament. The reason of such high increase in the temperature is that the velocity of air at the area is very low which limits the transfer of temperature through convection. Secondly, in the same symmetry plane, we observe a large areas of the flow behind the ligaments that have the uniform temperature. This is due to the re-circulation in the flow velocity that enhances mixing and homogenization of temperature.

6.1.3 Velocity Fields

Figure 6.6 shows the velocity magnitude vectors and contours at different cross-sections. Observing the velocity contours and vectors at the centerline we notice the huge increase in velocity while passing through the openings of the unit cell. The maximum velocity is approximately three times the superficial velocity where $V_{in} = 10.6 m/s$ and the maximum velocity is $V_{max} = 28.8 m/s$. The effect created is similar to jetting effect. We can notice two recirculating flow areas just below and above the jetting area. Another notice is the increase of average velocity by 30% from $10.6\,m/s$ to $13.8\,m/s$ between the inlet and the outlet zones due to the expansion of air caused by heat addition which decreases its density.

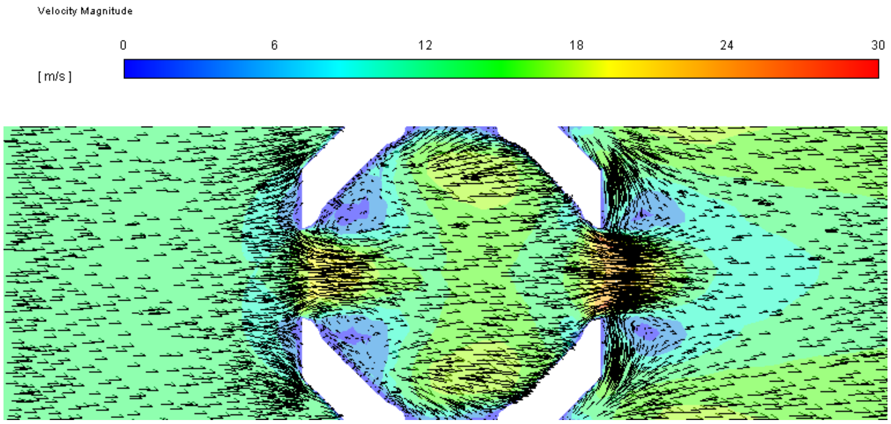

(a)Velocity magnitude contours on center plane

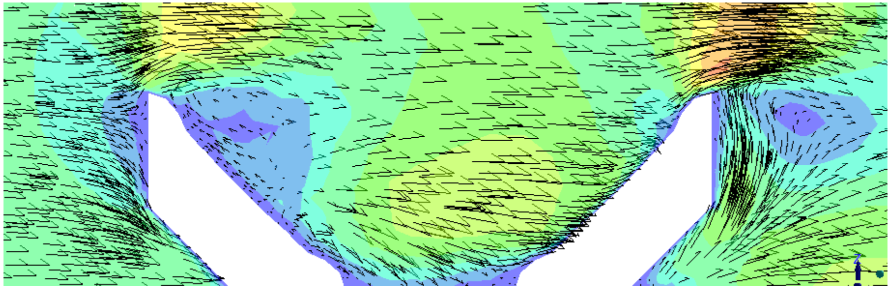

(b)Velocity magnitude contours on center plane enlarged

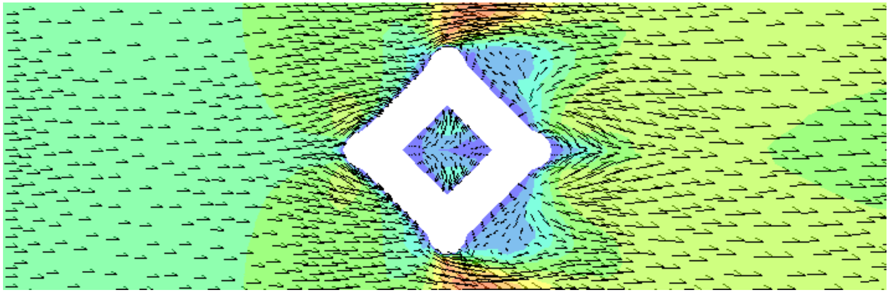

(c)Velocity magnitude contours on symmetry plane

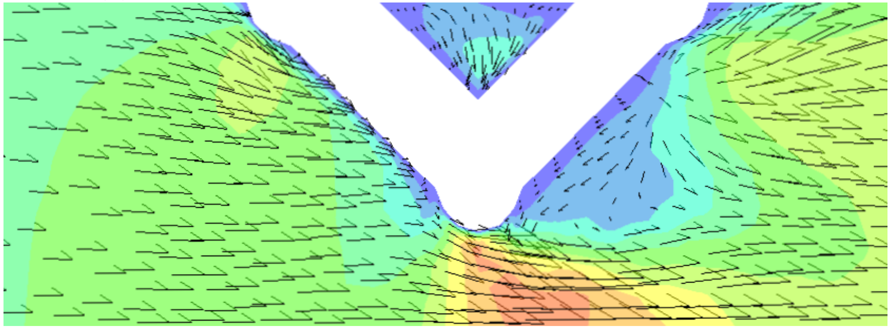

(d)Velocity magnitude contours on symmetry plane enlarged

Figure 6.6: Velocity magnitude contours in single cell model

6.1.4 Basic Case Overall Performance

The cell overall performance can be measured by three main parameters; the pressure drop ΔP, the volumetric heat transfer coefficient h_v and the cell efficiency η. Table 6.3 shows dimensional and non-dimensional results for both one cell and 2^3 cells.

Table 6.3: Basic Case Results

	Parameter	Value			% Diff.
		One Cell	2^3 Cells	$2^2 \times 3$ Cells	
1	$-\Delta P/\Delta x$ (kPa/m)	89.1	79.9	72.2	+23.4%
2	$h_v(\frac{W}{m^3 \cdot K})$	8.80×10^5	7.68×10^5	7.44×10^5	+18.3%
3	Nu	234	204	176	+33.0%
4	η	53.9 %	84.3 %	93.1 %	–
5	$\overline{T}_s(K)$	801	782	680	–
6	$T_{g,out}(K)$	386	434	447	–
7	Rad. Loss %	2 %	2 %	2 %	–

6.2 Parametric Study

In order to have a better understanding on the effects of the design and operation parameters on the results, a complete parametric study was done on a unit cell and an assembly of 2^3 multiple unit cells models. A part of the parametric study was done on the $2^2 \times 3$ geometry. The parametric study has all combinations of the following parameters and values.

Table 6.4: Parametric Design

	Parameter	**Values**	**Units**
1	k_s	1 - 10 - 100	$W/m^2 \cdot K$
2	α_s	0.1 - 0.5 - 0.9	
3	G	0.5 - 1.0 - 1.5 - 2.0 - 2.5	MW/m^2
4	m''	1.25 - 3.125 - 6.25 - 9.375 - 12.5	$kg/m^2 \cdot s$

A total number of 500 cases are modeled and the summary can be shown in the following sections.

6.2.1 Radiation Performance

Starting the parametric study results analysis similarly. Solar ray tracing method used in modeling radiation allows us to trace the solar irradiation on surfaces and at the inlet and outlet. The solar ray tracing method is independent of fluid flow solution and is only dependent on the geometrical and optical properties of the unit cell. Since we assume that the optical properties such as absorbtivity α_s and reflectivvity ρ_s are independent of temperature, solar ray tracing formulas is solved in the problem initialization step, before solving the full energy equation. Additionally, ratio of absorbed I_{abs}, reflected I_{ref} and transmitted I_{tran} fluxes to the solar irradiation G does not change by changing the irradiation G, mass flux m'' or the thermal conductivity of the solids k_s. It only changes by changing the solids' surface absorbtivity α_s. However, the emitted radiation I_e is not solved by the solar ray tracing method since it requires the solution of the energy equation

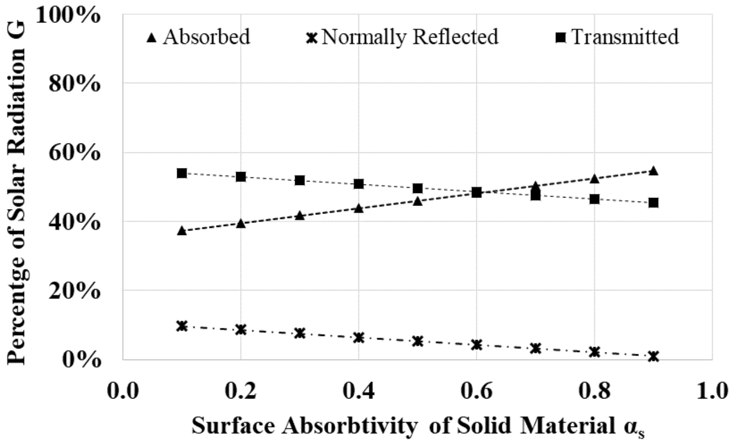

(a) One Cell

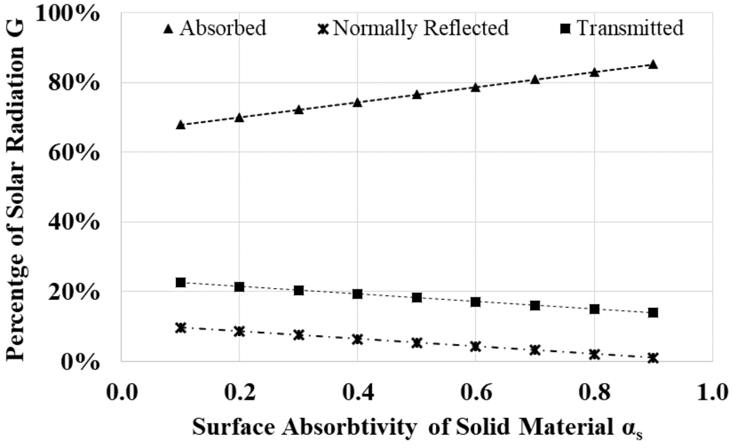

(b) 2^3 Cells

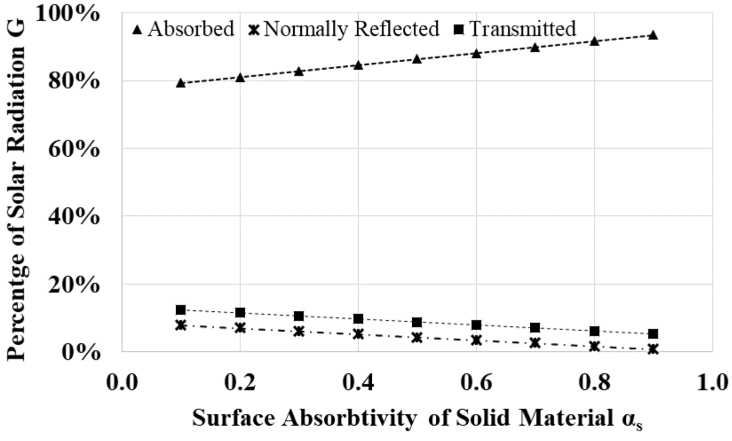

(c) $2^2 \times 3$ Cells

Figure 6.7: Effect of solid phase surface absorbtivity α_s on absorbed, transmitted and reflected fractions of solar radiation G.

to obtain surface temperatures.

The solution of solar ray tracing equations shown in Fig.6.7 shows the strong relation between the maximum absorbed percentage of incident radiation I_{abs} and the ratio of the projection area of the solids on the inlet area to the inlet area. Since the percentage of projection area of one cell is 65.4 % and for 2^3 cells is 94.1%, the maximum absorbed percentage of solar radiation can be calculated by $\%Area\ projection \times \alpha_s$ which gives us a value of 58.9% for a unit cell and 84.7% for 2^3 cells with both $\alpha_s = 0.9$. However this formula does not apply for lower values of α_s since larger portion of solar radiation is absorbed after a reflection or multiple reflection from the ligaments rather than directly absorbed.

Another noticeable feature of the solar ray tracing results is the unaffected normally reflected portion of solar radiation by the addition of multiple unit cells. This indicates that the normally reflected radiation from the 2^3 cells model is dominated by the first cell in the radiation direction. This can be explained by the nature of the geometry which consists of circular ligaments which reflect the incident radiation diffusely in all directions. Therefore, the addition of one unit cell only introduces circular ligaments that reflects the radiation diffusely and does not effectively contribute to the normally reflected portion of radiation. Hence the main part of the normally reflected radiation is reflected from the flat surfaces which creates the face of the unit cell.

Transmitted part of incident radiation can be divided into two parts;

- **Directly transmitted:** which is the part of radiation rays that goes from the inlet to the outlet straightly without facing any solids surface in its path.

- **Indirectly transmitted:** which is the part of radiation rays that went from the inlet to the outlet through multiple reflections against the solid surfaces.

The minimum amount of transmitted radiation is the directly transmitted radiation. It can be also calculated from the ratio of projection area of the solids on the inlet area to the inlet area. Where the percentage of directly transmitted radiation is equal to $1 - Projection\ Area\ Percentage$ which gives us a value of 34.6% for a unit cell and 5.9% for 2^3 cells. The directly transmitted radiation is only a function of the geometry and it is not affected by the surface properties of the material. Therefore, we can justify the increase of transmitted fraction of incident radiation - although the total frontal area of the model is the same - by the increase of indirectly transmitted radiation with increasing surface reflectivity ie; decreasing surface absorbtivity α_s.

We notice that the summation of the three components of the radiation equals 100%. This assures the convergence of the radiation intensity since we know that no radiation is scattered from section 6.1.1.

6.2.2 Efficiency

The cell efficiency is defined by Eq.5.11 as the ability of the system to transfer the incoming radiation energy to the fluid. The only sources of losses in the cell are radiation losses. Radiation losses are either direct through inability of the cell to capture the incoming radiation by means of reflection or transmission or indirect through inability to sustain absorbed radiation by means of radiation emission. However, transmitted radiation and emitted radiation to the backside of the system will be captured by other system components, and therefore will not be direct losses. Therefore, the cell losses reported are the reflected radiation and the emission radiation to the front side. In this subsection, efficiency and radiation losses are presented.

The general trend-line of the efficiency η is deceasing with the increase of specific energy as seen in Fig.6.8. The basic explanation for this trend is the increase in both direct and indirect radiation losses at higher specific energy values. In addition, by increasing the specific energy, the increase of indirect radiation losses is greater than the increase in convection heat transfer to the air. For example, design points 64, 73 and 154 from Table.B by doubling the intensity we notice that the radiation losses increases by 5 folds. However, doubling the mass flux increases the total enthalpy change by only 8%.

We also notice that high absorbtivity surfaces have higher efficiency while the specific energy is lower than $800kJ/kg$ for a single cell or $600kJ/kg$ for 2^3 cells and lower efficiency for higher specific energy levels. In the lower specific energy levels, unit cells with higher absorbtivity surfaces can absorb higher amounts of energy without affecting its radiation losses. A critical specific energy region between $800kJ/kg$ and $1,200kJ/kg$ for a single cell or between $500kJ/kg$ and $700kJ/kg$ for 2^3 cells exists where higher surface absorbtivity becomes a disadvantage due to its higher radiation losses due to higher emissions. The difference in the critical

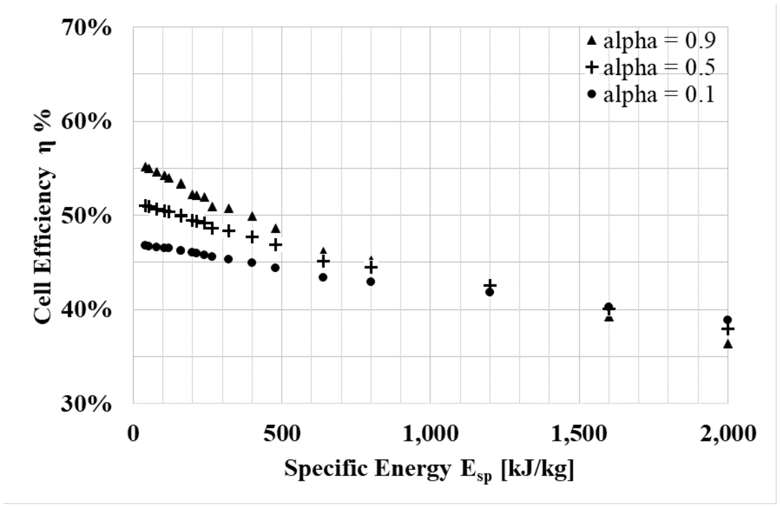

(a) One Cell

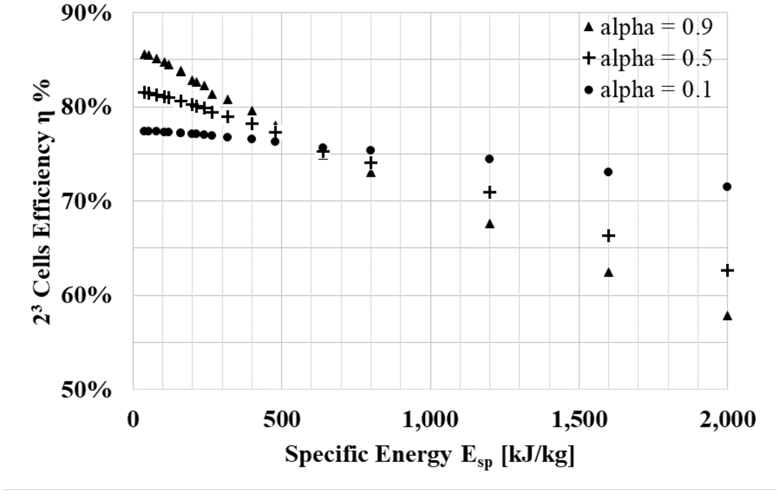

(b) 2^3 Cells

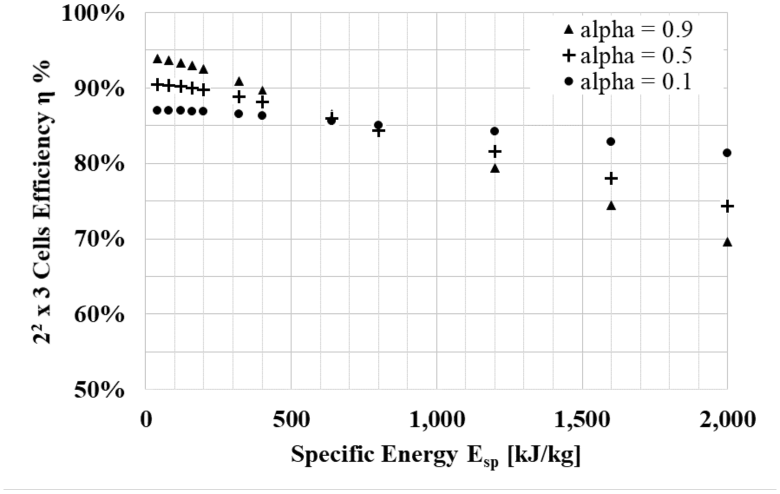

(c) $2^2 \times 3$ Cells

Figure 6.8: Efficiency Vs Specific Energy

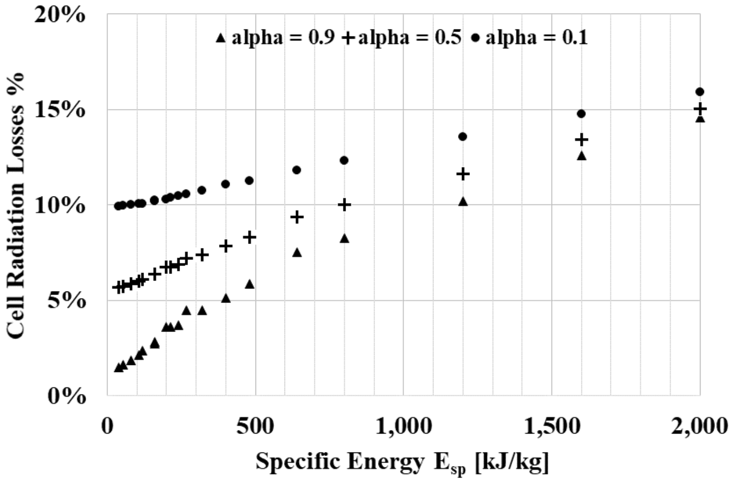

(a) One Cell

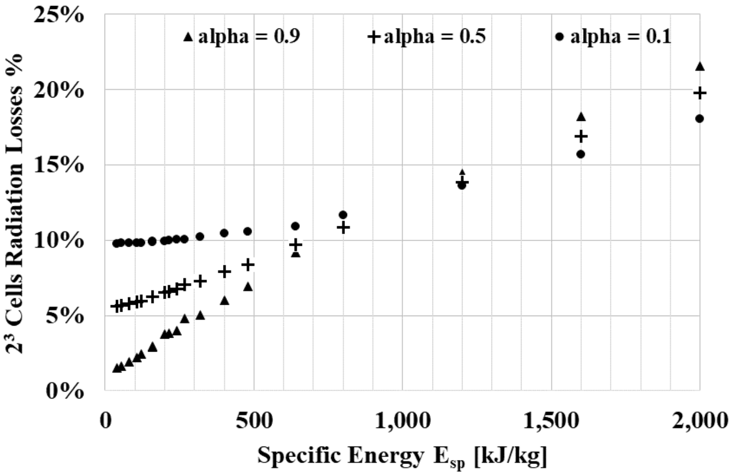

(b) 2^3 Cells

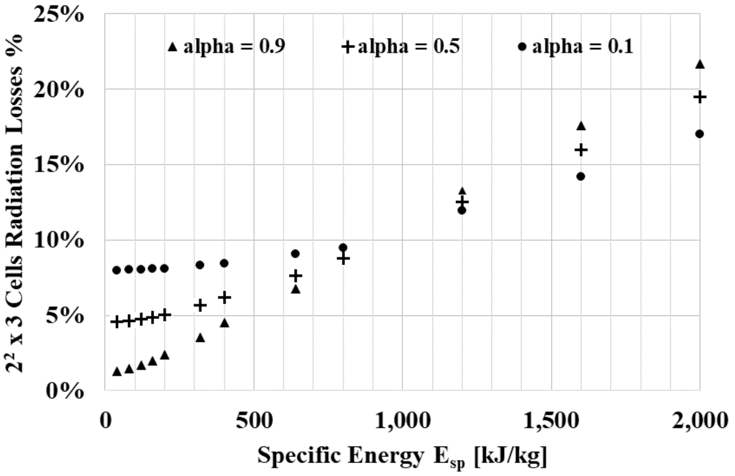

(c) $2^2 \times 3$ Cells

Figure 6.9: Radiation Losses Vs Specific Energy

specific energy level between one cell and 2^3 cell is due to the difference in the main cause of inefficiency between the two models. While direct radiation losses are the main cause of inefficiency in single cell model, indirect radiation the main cause of inefficiency in 2^3 cells model. However, most solar absorbers used commercially are optically thick, which means they do not allow any radiation to be transmitted directly through their thickness. Therefore, direct losses are reduced and the indirect losses becomes more important. Hence, the results obtained from multiple cells models are considered more realistic and conclusions should be made based on their results.

Although higher absorbtivity materials have less efficiency for specific energies larger than $600 kJ/kg$ it can be used efficiently upto specific energy values of $1,000 kJ/kg$ where the radiation losses becomes larger than low absorbtivity materials. In designing solar absorbers, the critical specific energy characteristic can be used by placing two foam materials on top of each other; a highly reflective foam in area subjected to specific energy of $2,000 kJ/kg$ or more - where radiation losses from highly reflective materials become less- , and a highly absorbing foam elsewhere. Up to the knowledge of the author, this critical value and its usefulness has is new to the literature.

The effect of solid thermal conductivity k_s on the cell efficiency η is less than 3%. Therefore it is not plotted.

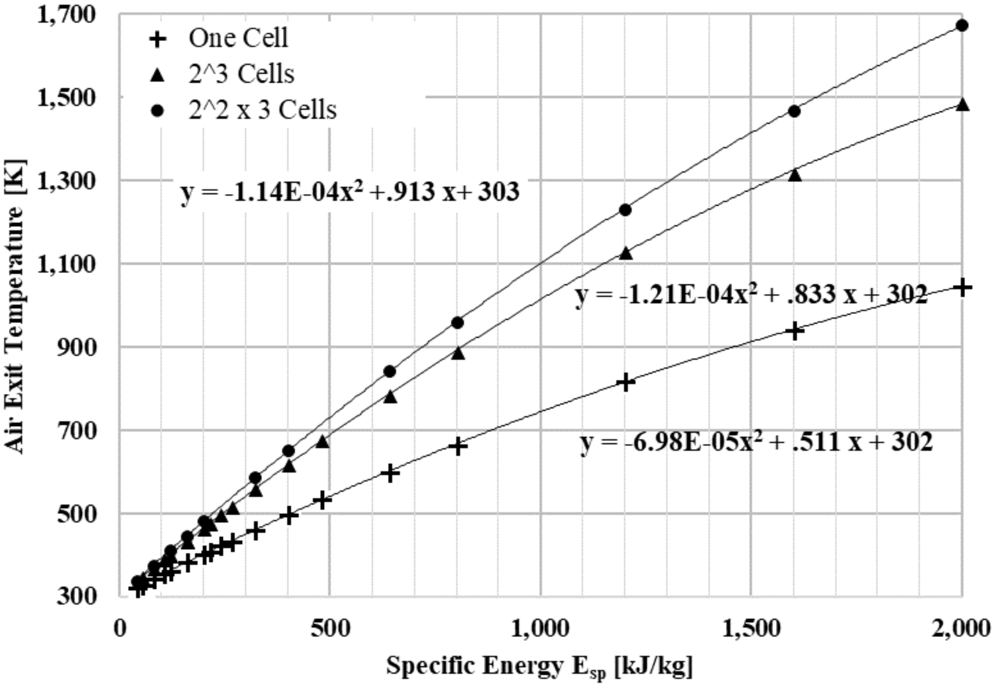

Figure 6.10: Air Exit Temperature Vs Specific Energy

6.2.3 Air Outlet Temperature

The main purpose of using ceramic foams in volumetric solar absorber is to heat the passing fluid, mainly air, usually to the highest possible temperature. Therefore the temperature of air after passing the foam is considered the most important parameter in evaluating the performance of a solar absorber. Figure 6.10 shows the strong dependency of air exit temperature $\overline{T}_{g,out}$ on the specific energy E_{SP}. The plot is given at $\alpha_s = 0.5$ and $k_s = 10 W/m \cdot K$. However all the other properties combination gives result within $+2\% \; -7\%$. Therefore the following formula is proposed to calculate the air exit temperature for $2^2 \times 3$ unit cells model with inlet temperature $T_{in} = 300 \; K$:

$$\overline{T}_{g,out} = -1.14 \times 10^{-4}\, E_{SP}^2 + .913 E_{SP} + 303 \qquad (6.1)$$

Equations such as the proposed equation are very useful in designing solar absorbers for a specific application where a certain temperature fluid exit temperature is desired in terms of specifying the required specific energy to achieve desired temperature.

6.2.4 Pressure Drop

Five extra cases were conducted for each geometry without any thermal load - Solar radiation - to obtain the fluid flow characteristics of the unit cell. Pressure drop was calculated according to Eq.5.12. Results are plotted in Fig.6.11 and a parabolic fit equations are shown. The single cell model has higher pressure drop coefficient due to the entrance effect. Specific permeability, and inertial resistance factor were calculated for a single cell model according to Darcy-Forchheimer Eq.2.1 and found to be $6.68 \times 10^{-8}\, m^{-1}$ and $968\, m^{-2}$ respectively. The results agreed well with previously derived correlation by Wu et al. based on experimental and numerical studies [2]. The 2^3 cells model results are at most 9% less than the derived correlation. The single cell model tends to overestimate the pressure drop $-\Delta P/\Delta x$ by an average value of 32% when compared to the 2^3 cells model.

However, it should be noted that the this pressure drop is only due to viscous forces. In solar absorbers; there will be static pressure loss due to the heat addition to the compressible air that passes through the heated ceramic foam. This pressure

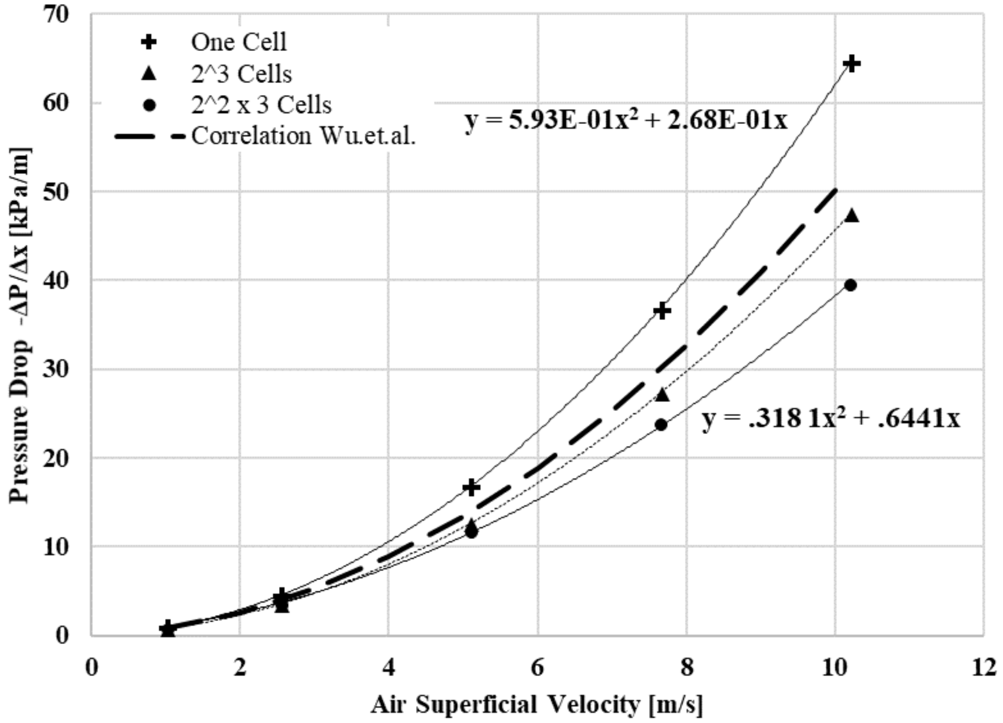

(a) Dimensional form

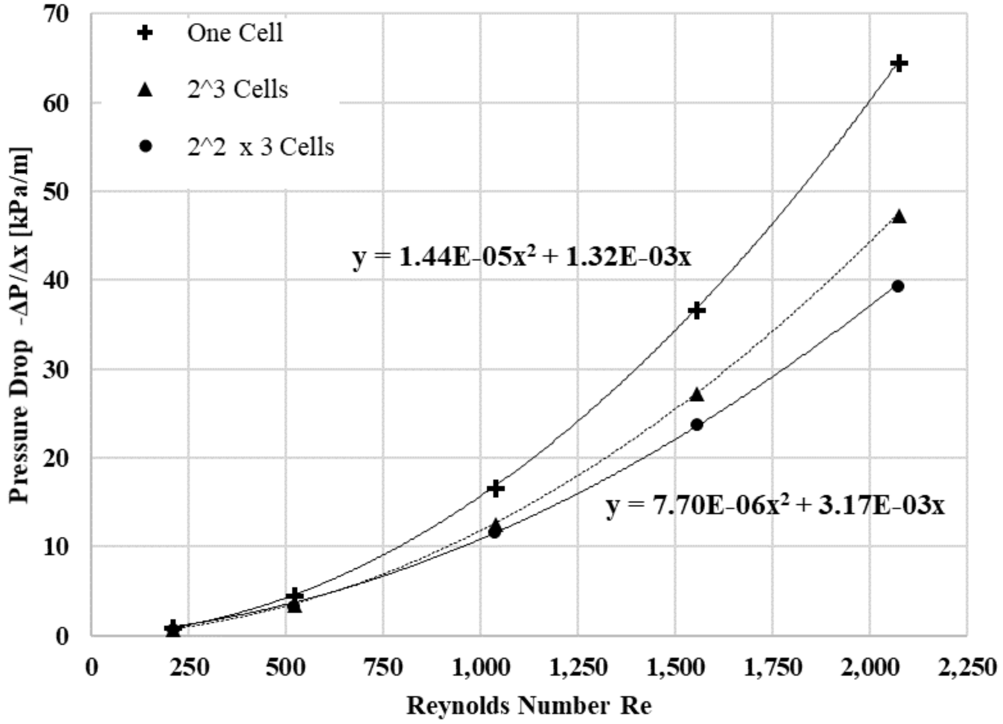

(b) Non-Dimensional form

Figure 6.11: Pressure drop in dimensional and non-dimensional forms

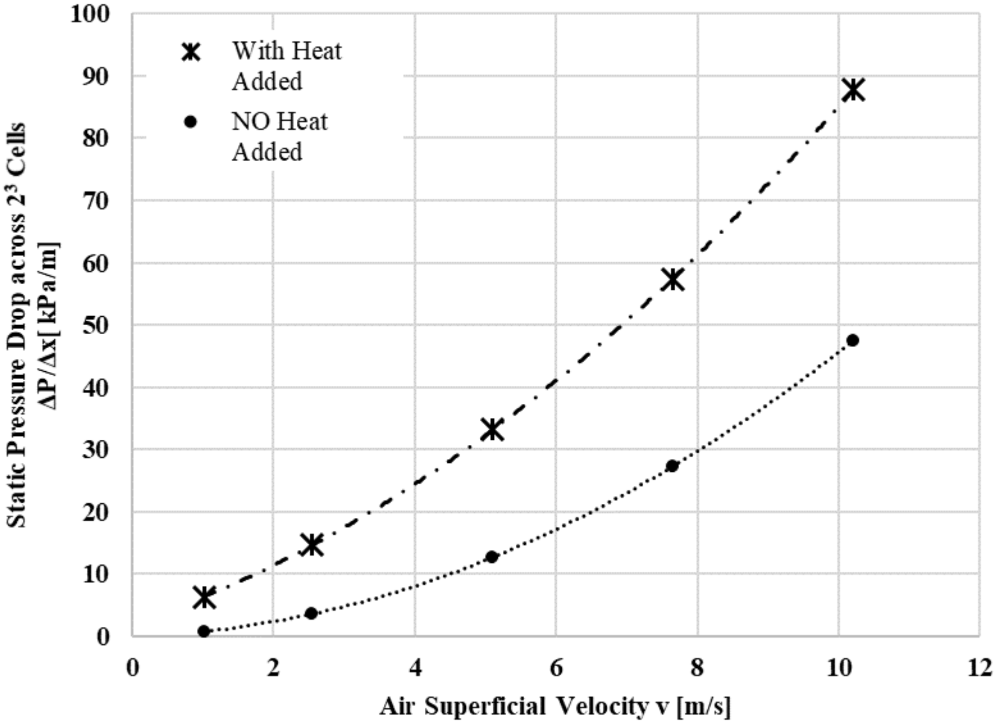

Figure 6.12: Pressure drop across 2^3 cells with heat addition.

loss contributes significantly to the static pressure loss. However, its calculation is undertaken in the energy and continuity equations. Figure 6.12 shows that pressure drop due to the heat addition may contribute upto 45% of the total static pressure loss. Therefore, the effect of heat addition must be considered while calculating the pressure loss for the solar absorber in order to select an appropriate compressor or a blower that can supply high enough pressure such that the pressure at the exit will not become vacuum pressure.

6.2.5 Volumetric Heat Transfer Coefficient

Figure 6.13 shows the average dimensional and non-dimensional values of volumetric heat transfer coefficient calculated by Eq.5.13, 5.15 for both one cell and

2^3 cells vs the superficial air velocity and Reynolds number. The figure shows that h_v depends mainly on the superficial velocity of the fluid, but is also strongly affected by other parameters as seen in Fig.6.14.

The second main parameter that affects h_v is the difference between the averages of air and ligaments temperatures $\overline{T}_s$ & $\overline{T}_g$. However, since $\overline{T}_{g,c}$ is mainly affected by the constant air inlet temperature of $300^{\circ}K$, h_v becomes dependent on $\overline{T}_s$. The volumetric heat transfer coefficient of one cell is higher 2^3 cells by an average of 20% due to entrance effect.

The results obtained from this section are validated against published numerical studies. Figure 6.14 shows the maximum and minimum Nusselt number vs Reynold's number compared with the correlation obtained by Wu et.al. [5]. The results shows very good agreement between this works results and previously derived correlation. However, the derived correlation was only obtained for a maximum $Re = 800$ and it was extrapolated to extend to our range. Therefore, the difference in the extrapolated range is larger.

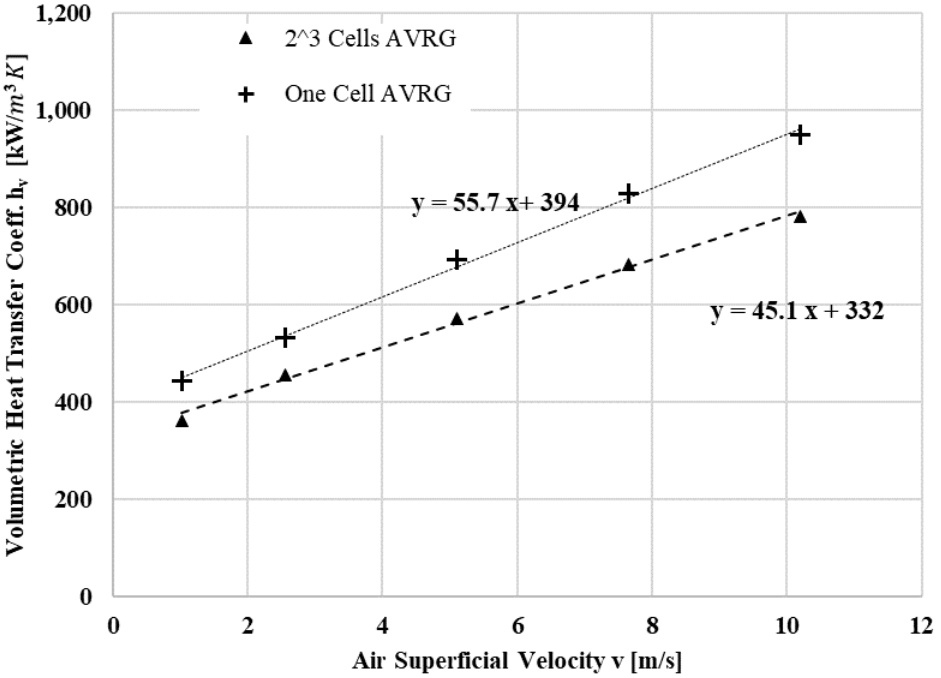

(a) Dimensional form

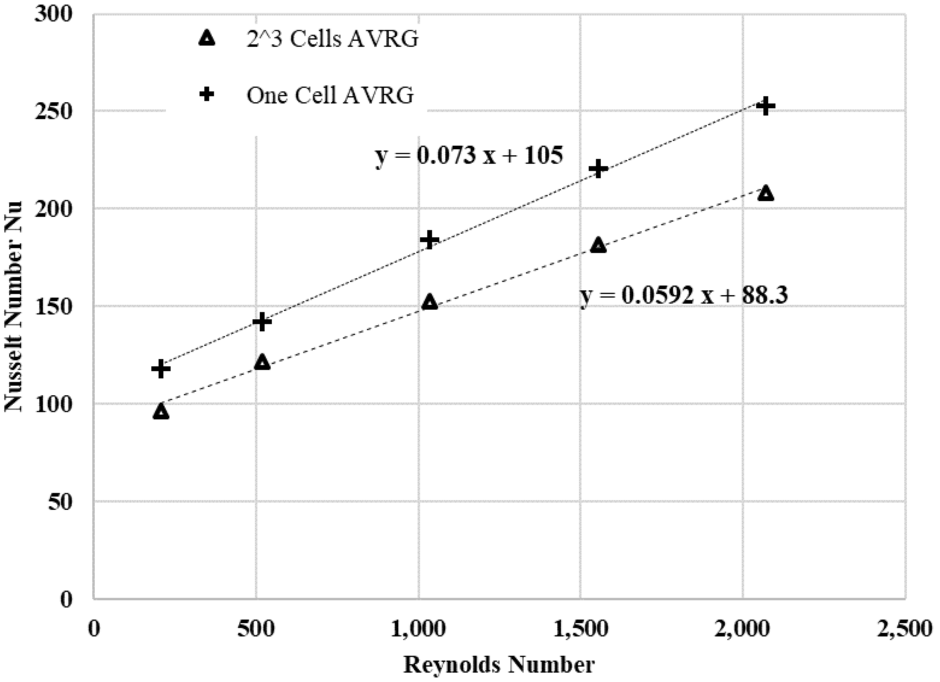

(b) Non-Dimensional form

Figure 6.13: Volumetric heat transfer coefficient in dimensional and non-dimensional formats.

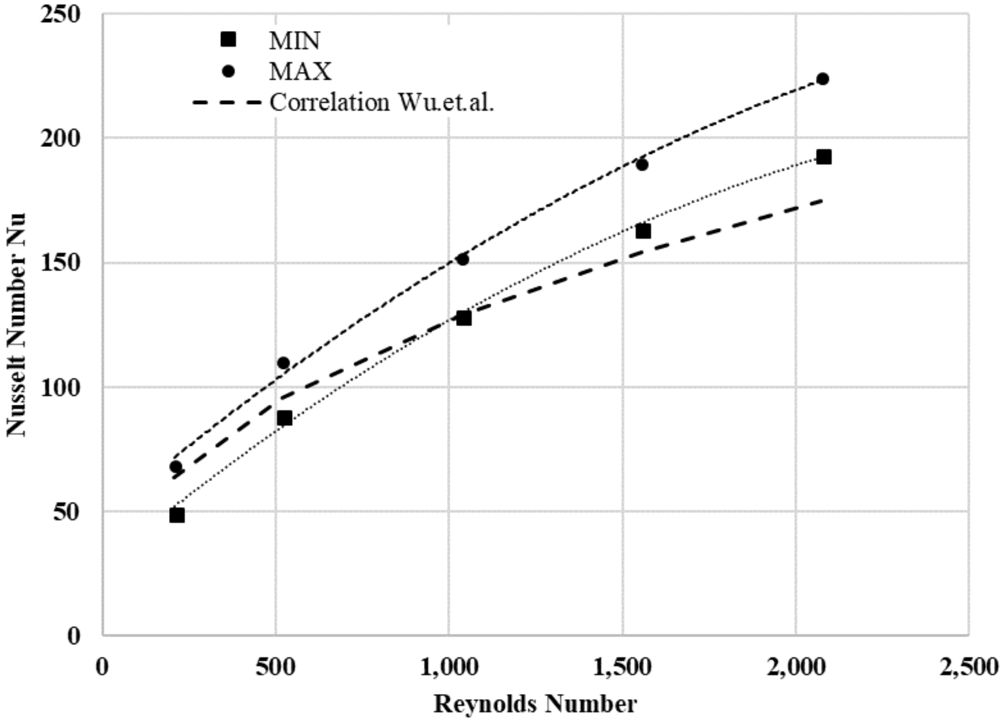

Figure 6.14: Maximum and minimum volumetric heat transfer coefficient for $2^2 \times 3$ unit cells.

CHAPTER 7

CONCLUSIONS

This chapter presents the main conclusions of the thesis including the major findings. The chapter also contains a recommendation section for future research in the field.

7.1 Conclusions

This thesis investigates the fluid flow and the heat transfer in ceramic foams used for high concentration solar receivers. The conducted literature review showed that using a numerical approach with simplified foam geometry gives accurate flow and heat transfer results without expensive computational cost and time. Therefore, a truncated octahedron strut consisting of circular beams -ligaments- was uses to generate the basic unit cell shape and to build two different multiple unit cells models.

A basic case simulation with solid ligaments thermal conductivity of $k_s = 100\, W/m \cdot K$ and surface absorbtivity of $\alpha_s = 0.9$ is subjected to an irradiation of $G = 2\ MW/m^2$ and a mass flux of air of $m'' = 12.5\ kg/m^2 \cdot s$. Radiation intensities, temperature profiles and flow pattern and vectors are thoroughly presented. The average air temperature at the outlet was found to be $T_{g,out} = 386\ K$ and the cell efficiency was $\eta = 58.9\%$ for a single unit cell model and $T_{g,out} = 447\ K\ \eta = 93.1\%$ for $2^2 \times 3$ unit cells model.

A parametric study consisting of 450 design points from different combinations of solids thermal conductivity k_s, surface emmisivity ϵ_s, mass fluxes m'' and solar irradiation G was conducted for models of different number of unit cells.A decline in the models' efficiency is observed with increasing specific energy. A critical value of the specific energy for a single cell model is found to be around $1MJ/kg$ where higher solid surface absorbtivity becomes a disadvantage. This critical value occurs at lower specific energy levels, between $0.5 - 0.6MJ/kg$ for multiple unit cells models. Further, pressure drop and volumetric heat transfer coefficient relations with flowrate and Reynolds number were obtained. The relations were found to be with good accuracy with published references.

Based on the work done; the following conclusions are made:

1. The unit cell approach is a simplified method that can be used to study the fluid flow and heat transfer in porous media and can give accurate results when compared to experimental methods.

2. The introduced ratio of radiation intensity flux to mass flow rate flux proved to be the main affecting parameter on the performance of ceramic foams.

3. The volumetric heat transfer coefficient is strongly affected by solid phase

temperature. Therefore, the use of its published values should be limited to the same range of temperatures.

4. The surface reflectivity was found to have much greater effect on the cell efficiency than the thermal conductivity. However, the thermal conductivity plays the major role in the temperature distribution within the cell and the temperature gradients within the ligaments.

7.2 Recommendations for Future Work

Based on the knowledge and experience from this work, this list of recommendations is proposed:

1. The performance of the unit cell should be obtained at many different orientations with respect to the fluid flow and the radiation intensity. A statistical method might me useful in obtaining the average cell property at a random orientation.
2. Similar Unit cell study should be done to study the effect of porosity and pore size on the results.
3. A separate study should be done to determine the size of the multiple unit cell model required to get the actual properties of the foam.
4. A detailed comparison with Local-Thermal-Non-Equilibrium (LTNE) should be done. Multiple correlations can be derived to relate maximum and minimum unit cell values to its average values used in LTNE approach.

5. Since many of the air properties depend on the pressure; the effect of operating the setup at elevated air pressure should be studied.

6. The effect of using a participating gas like carbon dioxide CO_2 or steam H_2O should be evaluated.

7. The effect of reversing the flow direction to be opposite to the radiation flux can be studied.

8. For a better simulation of the actual physical problem, variable intensity profile should be applied to the model. Its effect on the performance should be evaluated.

9. A thermal stress analysis can be carried out based on the temperature gradients in the ligaments to estimate ability of different materials to withstand the operation conditions in concentrated solar receivers without cracking.

Appendices

APPENDIX A

CASE AND DATA FILES FROM FLUENT

```
Fluent
Version: 3d, dp, pbns, rngke (3d, double precision, pressure-based, RNG k-epsilon)
Release: 18.2.0
Title:

Models
------

   Model                              Settings
   -----------------------------------------------------------------
   Space                              3D
   Time                               Steady
   Viscous                            RNG k-epsilon turbulence model
   Wall Treatment                     Enhanced Wall Treatment
   RNG Differential Viscosity Model   Disabled
   RNG Swirl Dominated Flow Option    Disabled
   Heat Transfer                      Enabled
   Solidification and Melting         Disabled
   Radiation                          Surface to Surface
   Species                            Disabled
   Coupled Dispersed Phase            Disabled
   NOx Pollutants                     Disabled
   SOx Pollutants                     Disabled
   Soot                               Disabled
   Mercury Pollutants                 Disabled

Material Properties
-------------------

   Material: air (fluid)

      Property                        Units     Method       Value(s)
      -------------------------------------------------------------------------------
---------------------------------------------------------
      Density                         kg/m3     ideal-gas
      Cp (Specific Heat)              j/kg-k    polynomial   (300 1005) (600 1051)
(900 1121) (1200 1175) (1500 1211)
      Thermal Conductivity            w/m-k     polynomial   (300 0.02624) (600
0.04661) (900 0.06276) (1200 0.0764) (1500 0.08831)
      Viscosity                       kg/m-s    polynomial   (300 1.846e-05) (600
3.017e-05) (900 3.897e-05) (1200 4.626e-05) (1500 5.264e-05)
      Molecular Weight                kg/kmol   constant     28.966
      Thermal Expansion Coefficient   1/k       constant     0
      Speed of Sound                  m/s       none

   Material: aluminum (solid)

      Property               Units    Method                 Value(s)
      ---------------------------------------------------------------
      Density                kg/m3    constant               2719
      Cp (Specific Heat)     j/kg-k   constant               871
      Thermal Conductivity   w/m-k    Thermal Conductivity   #f

Cell Zone Conditions
--------------------

   Zones

      name           id   type
      -------------------------
      fluid_domail   6    fluid
      ligaments      7    solid

   Setup Conditions

      fluid_domail
```

```
         Condition       Value
         ---------------------
         Frame Motion?   no
         Mesh Motion?    no

      ligaments

         Condition       Value
         ---------------------
         Frame Motion?   no
         Mesh Motion?    no

Boundary Conditions
-------------------

   Zones

      name                                 id   type
      ---------------------------------------------------------
      wall-ligaments                       9    symmetry
      wall-fluid_domail                    8    symmetry
      inlet                                10   mass-flow-inlet
      wall-fluid_domail-ligaments          1    wall
      outlet                               11   pressure-outlet
      symmetry_ligaments                12   symmetry
      symmetry_fluid_domail             13   symmetry
      symmetry_ligaments                14   symmetry
      symmetry_fluid_domail             15   symmetry
      symmetry_-z-ligaments                16   symmetry
      symmetry_-z-fluid_domail             17   symmetry
      symmetry_-y-ligaments                18   symmetry
      symmetry_-y-fluid_domail             19   symmetry
      wall-fluid_domail-ligaments-shadow   5    wall

   Setup Conditions

      wall-ligaments

         Condition   Value
         -----------------

      wall-fluid_domail

         Condition   Value
         -----------------

      inlet

         Condition        Value
         -------------------------------------
         Mass Flow Rate   (parameter . real-3)

      wall-fluid_domail-ligaments

         Condition                       Value
         ----------------------------------------------------
         Thermal BC Type                 3
         Direct Visible (Absorptivity)   (parameter . real-4)
         Direct IR (Absorptivity)        (parameter . real-4)

      outlet

         Condition                                         Value
         ----------------------------------------------------------------------
         Specify targeted mass flow rate                   yes
         Targeted mass flow                                (parameter . real-3)
         Upper Limit of Absolute Pressure Value (pascal)   5000000
         Lower Limit of Absolute Pressure Value (pascal)   1
```

```
      symmetry_ligaments

         Condition   Value
         -----------------

      symmetry_fluid_domail

         Condition   Value
         -----------------

      symmetry_ligaments

         Condition   Value
         -----------------

      symmetry_fluid_domail

         Condition   Value
         -----------------

      symmetry_-z-ligaments

         Condition   Value
         -----------------

      symmetry_-z-fluid_domail

         Condition   Value
         -----------------

      symmetry_-y-ligaments

         Condition   Value
         -----------------

      symmetry_-y-fluid_domail

         Condition   Value
         -----------------

      wall-fluid_domail-ligaments-shadow

         Condition                       Value
         ----------------------------------------------------
         Thermal BC Type                 3
         Wall Motion                     0
         Shear Boundary Condition        0
         Internal Emissivity             (parameter . real-4)
         Critical Zone                   yes
         Direct Visible (Absorptivity)   (parameter . real-4)
         Direct IR (Absorptivity)        (parameter . real-4)

Solver Settings
---------------

   Equations

      Equation     Solved
      -------------------
      Flow         yes
      Turbulence   yes
      Energy       yes

   Numerics

      Numeric                         Enabled
      ---------------------------------------
```

```
   Absolute Velocity Formulation   yes

Relaxation

   Variable                     Relaxation Factor
   ----------------------------------------------
   Pressure                     0.3
   Density                      1
   Body Forces                  1
   Momentum                     0.7
   Turbulent Kinetic Energy     0.8
   Turbulent Dissipation Rate   0.8
   Turbulent Viscosity          1
   Energy                       1

Linear Solver

                                Solver     Termination   Residual Reduction
   Variable                     Type       Criterion     Tolerance
   ------------------------------------------------------------------------
   Pressure                     V-Cycle    0.1
   X-Momentum                   Flexible   0.1           0.7
   Y-Momentum                   Flexible   0.1           0.7
   Z-Momentum                   Flexible   0.1           0.7
   Turbulent Kinetic Energy     Flexible   0.1           0.7
   Turbulent Dissipation Rate   Flexible   0.1           0.7
   Energy                       F-Cycle    0.1

Pressure-Velocity Coupling

   Parameter   Value
   ------------------
   Type        SIMPLE

Discretization Scheme

   Variable                     Scheme
   ------------------------------------------------
   Pressure                     Second Order
   Density                      Second Order Upwind
   Momentum                     Third-Order MUSCL
   Turbulent Kinetic Energy     Third-Order MUSCL
   Turbulent Dissipation Rate   Third-Order MUSCL
   Energy                       Third-Order MUSCL

Solution Limits

   Quantity                         Limit
   ---------------------------------------
   Minimum Absolute Pressure        1
   Maximum Absolute Pressure        5e
   Minimum Temperature              1
   Maximum Temperature              5000
   Minimum Turb. Kinetic Energy     1e-14
   Minimum Turb. Dissipation Rate   1e-20
   Maximum Turb. Viscosity Ratio    100000
```

APPENDIX B

PARAMETRIC STUDY TABLES

Table B.1: One Unit Cell Parametric Study Results

N	k_s	ϵ	m''	G	$\overline{T}_g$	$\overline{T}_s$	$T_{s,max}$	$T_{s,min}$	T_{in}	T_{out}	$q_{rad,in}$	$q_{rad,out}$	ΔP	h_v
	$\frac{W}{m \cdot K}$		$\frac{kg}{m^2 \cdot s}$	$\frac{MW}{m^2}$	K	K	K	K	K	K	W	W	Pa	$\frac{kW}{m^3 \cdot K}$
1	100	0.9	12.5	2.5	382	909	1003	813	301	406	-0.29	-0.21	269	893
2	10	0.9	12.5	2.5	395	917	1251	571	301	404	-0.51	-0.21	271	883
3	1	0.9	12.5	2.5	399	917	1490	465	301	402	-0.71	-0.22	272	872
4	100	0.5	12.5	2.5	373	824	877	770	305	403	-0.19	-0.14	258	975
5	10	0.5	12.5	2.5	381	832	1028	629	305	402	-0.26	-0.13	260	968
6	1	0.5	12.5	2.5	384	839	1186	561	305	401	-0.33	-0.14	260	955
7	100	0.1	12.5	2.5	363	735	745	723	308	399	-0.11	-0.09	246	1,094
8	10	0.1	12.5	2.5	365	739	778	688	308	399	-0.11	-0.09	247	1,088
9	1	0.1	9.375	2.5	366	749	825	658	308	399	-0.12	-0.10	247	1,063
10	100	0.9	9.375	2.5	406	994	1086	898	301	438	-0.41	-0.30	172	785
11	10	0.9	9.375	2.5	421	1003	1333	647	301	435	-0.68	-0.29	174	773
12	1	0.9	9.375	2.5	426	1003	1569	523	301	432	-0.93	-0.31	175	760
13	100	0.5	9.375	2.5	396	901	952	847	306	435	-0.26	-0.21	163	859
14	10	0.5	9.375	2.5	405	910	1104	700	306	434	-0.36	-0.19	165	852
15	1	0.5	9.375	2.5	409	918	1263	622	306	433	-0.44	-0.19	166	838
16	100	0.1	9.375	2.5	383	802	811	791	311	430	-0.15	-0.13	154	963
17	10	0.1	9.375	2.5	385	806	841	755	311	430	-0.16	-0.13	155	958
18	1	0.1	6.25	2.5	387	817	887	722	311	430	-0.16	-0.14	155	936
19	100	0.9	6.25	2.5	448	1119	1207	1027	302	498	-0.65	-0.49	96	659
20	10	0.9	6.25	2.5	464	1127	1440	777	302	493	-0.98	-0.45	97	648
21	1	0.9	6.25	2.5	469	1125	1663	630	302	487	-1.28	-0.45	98	635
22	100	0.5	6.25	2.5	437	1017	1065	965	310	497	-0.42	-0.34	90	725
23	10	0.5	6.25	2.5	448	1027	1210	821	310	495	-0.55	-0.31	91	718
24	1	0.5	6.25	2.5	452	1037	1361	730	310	493	-0.66	-0.31	92	705
25	100	0.1	6.25	2.5	421	906	912	895	316	491	-0.25	-0.22	84	816
26	10	0.1	6.25	2.5	423	910	935	863	316	491	-0.26	-0.21	85	811
27	1	0.1	3.125	2.5	424	922	994	825	316	491	-0.26	-0.22	85	793
28	100	0.9	3.125	2.5	533	1309	1391	1222	305	655	-1.20	-0.90	38	515
29	10	0.9	3.125	2.5	550	1310	1596	979	305	644	-1.60	-0.79	39	510

Continued on next page

Table B.1 – *One Unit Cell Parametric Study Results Continued ...*

N	k_s	ϵ	m''	G	$\overline{T}_g$	$\overline{T}_s$	$T_{s,max}$	$T_{s,min}$	T_{in}	T_{out}	$q_{rad,in}$	$q_{rad,out}$	ΔP	h_v
	$\frac{W}{m\cdot K}$		$\frac{kg}{m^2\cdot s}$	$\frac{MW}{m^2}$	K	K	K	K	K	K	W	W	Pa	$\frac{kW}{m^3\cdot K}$
30	1	0.9	3.125	2.5	556	1305	1802	817	305	632	-1.99	-0.73	39	498
31	100	0.5	3.125	2.5	525	1205	1247	1157	321	661	-0.83	-0.65	36	573
32	10	0.5	3.125	2.5	537	1212	1371	1021	321	657	-0.99	-0.58	36	570
33	1	0.5	3.125	2.5	542	1221	1507	925	321	653	-1.13	-0.56	37	559
34	100	0.1	3.125	2.5	503	1085	1087	1079	328	656	-0.52	-0.42	33	644
35	10	0.1	3.125	2.5	504	1089	1104	1054	328	656	-0.53	-0.42	33	641
36	1	0.1	1.25	2.5	504	1102	1172	1011	328	655	-0.51	-0.43	33	627
37	100	0.9	1.25	2.5	718	1529	1602	1449	312	1017	-2.25	-1.33	14	413
38	10	0.9	1.25	2.5	738	1525	1771	1240	312	992	-2.70	-1.17	14	409
39	1	0.9	1.25	2.5	743	1517	1954	1101	312	966	-3.12	-1.04	14	399
40	100	0.5	1.25	2.5	718	1438	1472	1397	344	1056	-1.74	-0.84	13	473
41	10	0.5	1.25	2.5	731	1442	1565	1290	344	1047	-1.92	-0.77	13	472
42	1	0.5	1.25	2.5	736	1448	1679	1216	344	1038	-2.07	-0.73	13	464
43	100	0.1	1.25	2.5	683	1324	1328	1318	350	1068	-1.26	-0.40	12	535
44	10	0.1	1.25	2.5	681	1327	1348	1298	350	1069	-1.23	-0.41	12	533
45	1	0.1	12.5	2.5	679	1338	1409	1264	350	1069	-1.20	-0.45	12	522
46	100	0.9	12.5	2	368	801	877	723	301	386	-0.17	-0.12	252	880
47	10	0.9	12.5	2	379	810	1095	521	301	385	-0.30	-0.12	254	872
48	1	0.9	12.5	2	383	811	1307	430	301	383	-0.42	-0.13	255	865
49	100	0.5	12.5	2	360	729	772	685	304	383	-0.11	-0.09	242	961
50	10	0.5	12.5	2	367	737	902	569	304	383	-0.16	-0.08	244	954
51	1	0.5	12.5	2	370	742	1039	511	304	382	-0.20	-0.08	244	943
52	100	0.1	12.5	2	351	655	663	645	306	380	-0.07	-0.06	233	1,079
53	10	0.1	12.5	2	353	658	691	617	306	380	-0.07	-0.06	234	1,073
54	1	0.1	9.375	2	354	666	731	593	306	379	-0.07	-0.06	234	1,050
55	100	0.9	9.375	2	389	875	950	797	301	413	-0.24	-0.18	158	772
56	10	0.9	9.375	2	402	885	1172	584	301	411	-0.41	-0.17	161	763
57	1	0.9	9.375	2	407	886	1385	476	301	409	-0.56	-0.19	162	753
58	100	0.5	9.375	2	379	796	837	752	305	410	-0.16	-0.12	151	844
59	10	0.5	9.375	2	387	804	970	628	305	409	-0.22	-0.11	153	838

Continued on next page

Table B.1 – *One Unit Cell Parametric Study Results Continued ...*

N	k_s	ϵ	m''	G	$\overline{T}_g$	$\overline{T}_s$	$T_{s,max}$	$T_{s,min}$	T_{in}	T_{out}	$q_{rad,in}$	$q_{rad,out}$	ΔP	h_v
	$\frac{W}{m \cdot K}$		$\frac{kg}{m^2 \cdot s}$	$\frac{MW}{m^2}$	K	K	K	K	K	K	W	W	Pa	$\frac{kW}{m^3 \cdot K}$
60	1	0.5	9.375	2	391	811	1111	560	305	408	-0.27	-0.12	154	826
61	100	0.1	9.375	2	369	712	720	703	309	405	-0.09	-0.08	144	946
62	10	0.1	9.375	2	370	716	746	674	309	405	-0.10	-0.08	144	941
63	1	0.1	6.25	2	371	724	785	646	309	405	-0.10	-0.08	144	921
64	100	0.9	6.25	2	426	988	1060	912	302	464	-0.39	-0.30	87	648
65	10	0.9	6.25	2	441	998	1275	697	302	460	-0.60	-0.28	89	638
66	1	0.9	6.25	2	447	1000	1481	567	302	456	-0.80	-0.28	89	627
67	100	0.5	6.25	2	415	898	938	856	308	461	-0.25	-0.20	82	711
68	10	0.5	6.25	2	425	908	1068	731	308	460	-0.33	-0.19	83	705
69	1	0.5	6.25	2	430	917	1206	651	308	458	-0.40	-0.19	84	693
70	100	0.1	6.25	2	401	802	808	794	313	456	-0.15	-0.13	77	798
71	10	0.1	6.25	2	403	806	828	767	313	456	-0.16	-0.13	77	794
72	1	0.1	3.125	2	404	816	876	735	313	456	-0.16	-0.13	77	777
73	100	0.9	3.125	2	503	1171	1238	1099	304	599	-0.76	-0.58	34	502
74	10	0.9	3.125	2	520	1175	1431	885	304	591	-1.03	-0.51	35	498
75	1	0.9	3.125	2	527	1173	1620	733	304	582	-1.30	-0.48	35	488
76	100	0.5	3.125	2	494	1075	1110	1036	318	601	-0.52	-0.41	32	555
77	10	0.5	3.125	2	505	1083	1224	917	318	598	-0.63	-0.37	33	553
78	1	0.5	3.125	2	511	1092	1349	825	318	595	-0.73	-0.36	33	544
79	100	0.1	3.125	2	476	968	969	963	325	595	-0.33	-0.26	30	624
80	10	0.1	3.125	2	477	971	983	942	325	595	-0.33	-0.26	30	621
81	1	0.1	1.25	2	477	981	1044	903	325	595	-0.33	-0.27	30	608
82	100	0.9	1.25	2	670	1386	1448	1321	309	921	-1.51	-0.91	12	401
83	10	0.9	1.25	2	691	1387	1610	1132	309	902	-1.84	-0.80	12	399
84	1	0.9	1.25	2	698	1381	1778	996	309	881	-2.15	-0.73	12	391
85	100	0.5	1.25	2	668	1299	1328	1266	339	947	-1.15	-0.58	12	455
86	10	0.5	1.25	2	681	1304	1417	1168	339	940	-1.28	-0.53	12	455
87	1	0.5	1.25	2	686	1311	1522	1094	339	933	-1.40	-0.50	12	448
88	100	0.1	1.25	2	637	1191	1194	1187	348	950	-0.82	-0.29	11	513
89	10	0.1	1.25	2	635	1193	1211	1169	348	951	-0.80	-0.29	11	511

Continued on next page

Table B.1 – *One Unit Cell Parametric Study Results Continued ...*

N	k_s	ϵ	m''	G	$\overline{T}_g$	$\overline{T}_s$	$T_{s,max}$	$T_{s,min}$	T_{in}	T_{out}	$q_{rad,in}$	$q_{rad,out}$	ΔP	h_v
	$\frac{W}{m \cdot K}$		$\frac{kg}{m^2 \cdot s}$	$\frac{MW}{m^2}$	K	K	K	K	K	K	W	W	Pa	$\frac{kW}{m^3 \cdot K}$
90	1	0.1	12.5	2	634	1202	1268	1139	348	951	-0.78	-0.32	11	501
91	100	0.9	12.5	1.5	353	686	744	627	301	365	-0.09	-0.07	234	866
92	10	0.9	12.5	1.5	362	695	923	469	301	365	-0.15	-0.06	235	859
93	1	0.9	12.5	1.5	365	696	1100	397	301	364	-0.22	-0.07	236	855
94	100	0.5	12.5	1.5	346	630	662	597	303	363	-0.06	-0.05	227	945
95	10	0.5	12.5	1.5	352	636	767	506	303	363	-0.08	-0.04	228	939
96	1	0.5	12.5	1.5	354	640	879	460	303	362	-0.10	-0.04	228	930
97	100	0.1	12.5	1.5	339	572	578	565	305	360	-0.04	-0.03	220	1,060
98	10	0.1	12.5	1.5	341	574	601	544	305	360	-0.04	-0.03	220	1,055
99	1	0.1	9.375	1.5	341	580	633	525	305	360	-0.04	-0.03	220	1,034
100	100	0.9	9.375	1.5	369	747	804	688	301	386	-0.13	-0.09	145	758
101	10	0.9	9.375	1.5	380	757	989	519	301	385	-0.21	-0.09	146	751
102	1	0.9	9.375	1.5	385	759	1174	430	301	384	-0.29	-0.10	148	745
103	100	0.5	9.375	1.5	361	683	715	650	304	383	-0.08	-0.07	139	827
104	10	0.5	9.375	1.5	368	691	824	553	304	383	-0.11	-0.06	140	822
105	1	0.5	9.375	1.5	371	696	941	498	304	383	-0.14	-0.06	141	813
106	100	0.1	9.375	1.5	353	618	623	611	307	380	-0.05	-0.04	134	927
107	10	0.1	9.375	1.5	354	620	644	589	307	380	-0.05	-0.04	134	923
108	1	0.1	6.25	1.5	355	627	676	567	307	380	-0.06	-0.04	134	904
109	100	0.9	6.25	1.5	400	842	898	783	301	426	-0.20	-0.15	78	634
110	10	0.9	6.25	1.5	414	854	1085	609	301	424	-0.32	-0.14	79	627
111	1	0.9	6.25	1.5	420	857	1268	501	301	422	-0.43	-0.15	80	618
112	100	0.5	6.25	1.5	390	768	798	736	306	423	-0.13	-0.11	74	694
113	10	0.5	6.25	1.5	399	777	908	635	306	423	-0.18	-0.10	75	689
114	1	0.5	6.25	1.5	404	785	1028	568	306	422	-0.22	-0.10	75	679
115	100	0.1	6.25	1.5	379	691	695	685	311	419	-0.08	-0.07	70	779
116	10	0.1	6.25	1.5	381	694	712	664	311	419	-0.09	-0.07	70	775
117	1	0.1	3.125	1.5	382	702	747	638	311	419	-0.09	-0.07	70	759
118	100	0.9	3.125	1.5	468	1009	1061	954	303	536	-0.41	-0.32	30	487
119	10	0.9	3.125	1.5	484	1017	1235	776	303	531	-0.57	-0.28	30	484

Continued on next page

Table B.1 – *One Unit Cell Parametric Study Results Continued ...*

N	k_s	ϵ	m''	G	$\overline{T}_g$	$\overline{T}_s$	$T_{s,max}$	$T_{s,min}$	T_{in}	T_{out}	$q_{rad,in}$	$q_{rad,out}$	ΔP	h_v
	$\frac{W}{m \cdot K}$		$\frac{kg}{m^2 \cdot s}$	$\frac{MW}{m^2}$	K	K	K	K	K	K	W	W	Pa	$\frac{kW}{m^3 \cdot K}$
120	1	0.9	3.125	1.5	492	1019	1407	640	303	525	-0.74	-0.28	31	476
121	100	0.5	3.125	1.5	458	926	953	897	314	535	-0.28	-0.22	28	535
122	10	0.5	3.125	1.5	468	934	1052	798	314	533	-0.35	-0.20	28	533
123	1	0.5	3.125	1.5	474	943	1164	715	314	531	-0.40	-0.20	29	526
124	100	0.1	3.125	1.5	443	835	836	831	322	530	-0.18	-0.14	26	601
125	10	0.1	3.125	1.5	444	837	847	815	322	530	-0.18	-0.14	26	599
126	1	0.1	1.25	1.5	445	846	898	783	322	530	-0.18	-0.15	26	587
127	100	0.9	1.25	1.5	612	1215	1263	1165	307	809	-0.89	-0.54	10	386
128	10	0.9	1.25	1.5	633	1220	1414	1003	307	795	-1.10	-0.48	11	385
129	1	0.9	1.25	1.5	642	1218	1568	873	307	779	-1.31	-0.45	11	379
130	100	0.5	1.25	1.5	606	1134	1156	1108	332	822	-0.67	-0.35	10	433
131	10	0.5	1.25	1.5	618	1140	1238	1025	332	817	-0.75	-0.32	10	433
132	1	0.5	1.25	1.5	625	1147	1334	953	332	812	-0.82	-0.30	10	427
133	100	0.1	1.25	1.5	582	1037	1039	1033	345	820	-0.47	-0.18	9	488
134	10	0.1	1.25	1.5	581	1038	1052	1019	345	821	-0.46	-0.18	9	485
135	1	0.1	12.5	1.5	580	1045	1102	994	345	821	-0.44	-0.19	9	476
136	100	0.9	12.5	1	336	565	604	526	300	344	-0.04	-0.03	216	848
137	10	0.9	12.5	1	343	572	734	416	300	344	-0.06	-0.03	217	843
138	1	0.9	12.5	1	346	573	867	364	300	343	-0.09	-0.03	217	843
139	100	0.5	12.5	1	332	526	547	504	302	342	-0.03	-0.02	211	925
140	10	0.5	12.5	1	335	530	622	441	302	342	-0.04	-0.02	211	920
141	1	0.5	12.5	1	337	533	704	408	302	342	-0.04	-0.02	212	914
142	100	0.1	12.5	1	327	485	490	481	303	340	-0.02	-0.01	206	1,040
143	10	0.1	12.5	1	328	487	506	466	303	340	-0.02	-0.01	206	1,036
144	1	0.1	9.375	1	328	490	529	453	303	340	-0.02	-0.01	206	1,017
145	100	0.9	9.375	1	348	609	648	569	301	358	-0.05	-0.04	130	739
146	10	0.9	9.375	1	356	617	785	450	301	358	-0.08	-0.04	132	735
147	1	0.9	9.375	1	360	620	927	385	301	357	-0.12	-0.04	132	733
148	100	0.5	9.375	1	342	564	586	542	303	356	-0.04	-0.03	127	806
149	10	0.5	9.375	1	347	570	664	474	303	356	-0.05	-0.03	127	802

Continued on next page

Table B.1 – *One Unit Cell Parametric Study Results Continued ...*

N	k_s	ϵ	m''	G	$\overline{T}_g$	$\overline{T}_s$	$T_{s,max}$	$T_{s,min}$	T_{in}	T_{out}	$q_{rad,in}$	$q_{rad,out}$	ΔP	h_v
	$\frac{W}{m \cdot K}$		$\frac{kg}{m^2 \cdot s}$	$\frac{MW}{m^2}$	K	K	K	K	K	K	W	W	Pa	$\frac{kW}{m^3 \cdot K}$
150	1	0.5	9.375	1	350	573	752	434	303	356	-0.06	-0.03	128	796
151	100	0.1	9.375	1	336	518	522	514	305	354	-0.02	-0.02	123	904
152	10	0.1	9.375	1	337	520	537	499	305	354	-0.03	-0.02	123	901
153	1	0.1	6.25	1	338	524	561	484	305	354	-0.03	-0.02	123	884
154	100	0.9	6.25	1	371	680	718	640	301	386	-0.08	-0.06	68	617
155	10	0.9	6.25	1	381	690	862	514	301	385	-0.13	-0.06	69	612
156	1	0.9	6.25	1	388	695	1012	432	301	384	-0.18	-0.06	69	607
157	100	0.5	6.25	1	363	626	647	605	304	384	-0.06	-0.04	65	674
158	10	0.5	6.25	1	369	633	729	533	304	383	-0.07	-0.04	65	670
159	1	0.5	6.25	1	373	639	823	482	304	383	-0.09	-0.04	66	663
160	100	0.1	6.25	1	355	572	575	568	307	381	-0.04	-0.03	62	755
161	10	0.1	6.25	1	356	574	588	553	307	381	-0.04	-0.03	62	752
162	1	0.1	3.125	1	357	579	610	535	307	381	-0.04	-0.03	62	738
163	100	0.9	3.125	1	425	818	853	780	302	465	-0.18	-0.13	25	468
164	10	0.9	3.125	1	439	828	994	648	302	463	-0.24	-0.12	25	466
165	1	0.9	3.125	1	447	833	1142	539	302	460	-0.32	-0.12	26	460
166	100	0.5	3.125	1	416	752	771	732	310	463	-0.12	-0.09	23	512
167	10	0.5	3.125	1	424	760	849	660	310	462	-0.15	-0.09	24	510
168	1	0.5	3.125	1	430	768	941	593	310	461	-0.18	-0.08	24	504
169	100	0.1	3.125	1	404	683	684	681	316	459	-0.08	-0.06	22	575
170	10	0.1	3.125	1	405	685	691	670	316	459	-0.08	-0.06	22	573
171	1	0.1	1.25	1	406	691	728	646	316	459	-0.08	-0.06	22	562
172	100	0.9	1.25	1	540	1001	1034	966	305	673	-0.40	-0.25	8	365
173	10	0.9	1.25	1	558	1009	1164	842	305	666	-0.51	-0.22	8	365
174	1	0.9	1.25	1	569	1012	1302	726	305	656	-0.62	-0.21	8	362
175	100	0.5	1.25	1	530	930	946	913	322	675	-0.30	-0.16	8	404
176	10	0.5	1.25	1	540	937	1014	849	322	673	-0.34	-0.15	8	404
177	1	0.5	1.25	1	547	944	1099	783	322	669	-0.38	-0.14	8	400
178	100	0.1	1.25	1	513	851	852	849	337	671	-0.21	-0.08	7	454
179	10	0.1	1.25	1	512	851	862	839	337	672	-0.21	-0.09	7	452

Continued on next page

Table B.1 – *One Unit Cell Parametric Study Results Continued ...*

N	k_s	ϵ	m''	G	$\overline{T}_g$	$\overline{T}_s$	$T_{s,max}$	$T_{s,min}$	T_{in}	T_{out}	$q_{rad,in}$	$q_{rad,out}$	ΔP	h_v
	$\frac{W}{m \cdot K}$		$\frac{kg}{m^2 \cdot s}$	$\frac{MW}{m^2}$	K	K	K	K	K	K	W	W	Pa	$\frac{kW}{m^3 \cdot K}$
180	1	0.1	12.5	1	511	857	901	819	337	672	-0.20	-0.09	7	444
181	100	0.9	12.5	0.5	319	437	457	417	300	322	-0.01	-0.01	197	828
182	10	0.9	12.5	0.5	322	441	527	360	300	322	-0.02	-0.01	197	821
183	1	0.9	12.5	0.5	324	442	603	331	300	322	-0.02	-0.01	198	825
184	100	0.5	12.5	0.5	316	416	427	405	301	321	-0.01	-0.01	195	906
185	10	0.5	12.5	0.5	318	418	467	372	301	321	-0.01	-0.01	195	900
186	1	0.5	12.5	0.5	319	420	513	355	301	321	-0.01	-0.01	195	896
187	100	0.1	12.5	0.5	314	395	397	392	302	320	-0.01	0.00	192	1,021
188	10	0.1	12.5	0.5	314	395	405	385	302	320	-0.01	0.00	192	1,017
189	1	0.1	9.375	0.5	314	397	418	379	302	320	-0.01	0.00	192	1,001
190	100	0.9	9.375	0.5	325	461	481	441	300	329	-0.01	-0.01	116	717
191	10	0.9	9.375	0.5	329	466	557	378	300	329	-0.02	-0.01	116	712
192	1	0.9	9.375	0.5	332	467	640	342	300	329	-0.03	-0.01	117	715
193	100	0.5	9.375	0.5	322	437	448	426	301	328	-0.01	-0.01	114	783
194	10	0.5	9.375	0.5	324	440	490	390	301	328	-0.01	-0.01	114	779
195	1	0.5	9.375	0.5	326	442	541	368	301	328	-0.02	-0.01	114	775
196	100	0.1	9.375	0.5	319	412	414	410	302	327	-0.01	-0.01	112	882
197	10	0.1	9.375	0.5	319	413	423	403	302	327	-0.01	-0.01	112	879
198	1	0.1	6.25	0.5	319	415	436	395	302	327	-0.01	-0.01	112	865
199	100	0.9	6.25	0.5	337	501	521	481	300	344	-0.02	-0.02	57	593
200	10	0.9	6.25	0.5	343	507	603	412	300	344	-0.03	-0.01	57	590
201	1	0.9	6.25	0.5	347	510	696	364	300	344	-0.04	-0.01	58	590
202	100	0.5	6.25	0.5	333	472	482	461	302	342	-0.02	-0.01	56	647
203	10	0.5	6.25	0.5	336	476	528	422	302	342	-0.02	-0.01	56	644
204	1	0.5	6.25	0.5	339	479	584	393	302	342	-0.02	-0.01	56	640
205	100	0.1	6.25	0.5	329	442	444	440	304	341	-0.01	-0.01	54	727
206	10	0.1	6.25	0.5	329	443	451	432	304	341	-0.01	-0.01	54	724
207	1	0.1	3.125	0.5	330	445	464	423	304	341	-0.01	-0.01	54	713
208	100	0.9	3.125	0.5	371	586	605	567	301	386	-0.04	-0.03	19	442
209	10	0.9	3.125	0.5	380	595	691	494	301	386	-0.06	-0.03	19	441

Continued on next page

Table B.1 – *One Unit Cell Parametric Study Results Continued ...*

N	k_s	ϵ	m''	G	$\overline{T}_g$	$\overline{T}_s$	$T_{s,max}$	$T_{s,min}$	T_{in}	T_{out}	$q_{rad,in}$	$q_{rad,out}$	ΔP	h_v
	$\frac{W}{m \cdot K}$		$\frac{kg}{m^2 \cdot s}$	$\frac{MW}{m^2}$	K	K	K	K	K	K	W	W	Pa	$\frac{kW}{m^3 \cdot K}$
210	1	0.9	3.125	0.5	387	600	795	426	301	385	-0.08	-0.03	20	439
211	100	0.5	3.125	0.5	364	548	557	537	305	384	-0.03	-0.02	18	482
212	10	0.5	3.125	0.5	369	553	604	497	305	384	-0.04	-0.02	19	481
213	1	0.5	3.125	0.5	373	558	664	457	305	384	-0.04	-0.02	19	477
214	100	0.1	3.125	0.5	357	508	508	506	309	382	-0.02	-0.02	18	541
215	10	0.1	3.125	0.5	357	508	512	501	309	382	-0.02	-0.02	18	540
216	1	0.1	1.25	0.5	358	511	532	488	309	382	-0.02	-0.02	18	531
217	100	0.9	1.25	0.5	443	716	733	699	302	505	-0.10	-0.06	6	334
218	10	0.9	1.25	0.5	455	725	819	625	302	503	-0.13	-0.06	6	336
219	1	0.9	1.25	0.5	466	732	928	542	302	499	-0.16	-0.06	6	335
220	100	0.5	1.25	0.5	433	668	676	659	312	501	-0.08	-0.04	5	365
221	10	0.5	1.25	0.5	439	673	719	621	312	501	-0.09	-0.04	5	366
222	1	0.5	1.25	0.5	446	679	780	574	312	500	-0.10	-0.04	5	364
223	100	0.1	1.25	0.5	421	616	617	615	320	497	-0.05	-0.02	5	409
224	10	0.1	1.25	0.5	420	616	621	610	320	497	-0.05	-0.02	5	407
225	1	0.1	1.25	0.5	420	619	645	598	320	497	-0.05	-0.03	5	400
226	100	0.9	3.125	0	300	300	300	300	300	300	0.00	0.00	178	-
227	100	0.9	6.25	0	300	300	300	300	300	300	0.00	0.00	101	-
228	100	0.9	9.375	0	300	300	300	300	300	300	0.00	0.00	46	-
229	100	0.9	12.5	0	300	300	300	300	300	300	0.00	0.00	13	-
230	100	0.9	1.25	0	300	300	300	300	300	300	0.00	0.00	3	-

Table B.2: 2^3 Cells Parametric Study Results

N	k_s	ϵ	m''	G	$\overline{T}_g$	$\overline{T}_s$	$T_{s,max}$	$T_{s,min}$	T_{in}	T_{out}	$q_{rad,in}$	$q_{rad,out}$	ΔP	h_v
	$\frac{W}{m \cdot K}$		$\frac{kg}{m^2 \cdot s}$	$\frac{MW}{m^2}$	K	K	K	K	K	K	W	W	Pa	$\frac{kW}{m^3 \cdot K}$
1	100	0.9	12.5	2.5	418	888	1070	749	300	466	-1.38	-0.70	493	786
2	10	0.9	12.5	2.5	423	893	1329	573	300	464	-2.15	-0.59	496	779
3	1	0.9	12.5	2.5	424	898	1578	466	300	462	-2.81	-0.58	496	764
4	100	0.5	12.5	2.5	410	839	941	754	300	465	-0.70	-0.45	483	829
5	10	0.5	12.5	2.5	414	845	1113	626	300	464	-0.91	-0.41	486	822
6	1	0.5	12.5	2.5	415	856	1303	542	300	464	-1.05	-0.42	485	802
7	100	0.1	12.5	2.5	402	788	811	759	300	464	-0.17	-0.13	473	884
8	10	0.1	12.5	2.5	403	792	885	684	300	463	-0.18	-0.13	473	876
9	1	0.1	9.375	2.5	404	807	1045	619	300	463	-0.19	-0.15	471	847
10	100	0.9	9.375	2.5	458	983	1158	841	300	517	-2.00	-1.07	322	694
11	10	0.9	9.375	2.5	464	988	1402	640	300	514	-2.97	-0.89	325	686
12	1	0.9	9.375	2.5	465	995	1652	509	300	512	-3.77	-0.88	323	671
13	100	0.5	9.375	2.5	449	930	1026	843	300	517	-1.04	-0.70	316	733
14	10	0.5	9.375	2.5	453	937	1188	697	300	517	-1.31	-0.63	317	725
15	1	0.5	9.375	2.5	455	951	1398	591	300	516	-1.50	-0.66	317	706
16	100	0.1	9.375	2.5	439	875	897	847	300	517	-0.27	-0.19	309	780
17	10	0.1	9.375	2.5	440	880	977	760	300	517	-0.27	-0.20	308	774
18	1	0.1	6.25	2.5	442	897	1142	676	300	517	-0.28	-0.23	307	747
19	100	0.9	6.25	2.5	534	1128	1287	986	300	613	-3.29	-1.91	186	593
20	10	0.9	6.25	2.5	539	1132	1503	750	300	609	-4.51	-1.59	188	586
21	1	0.9	6.25	2.5	539	1139	1757	573	300	604	-5.50	-1.54	187	570
22	100	0.5	6.25	2.5	524	1073	1156	988	300	618	-1.79	-1.25	183	628
23	10	0.5	6.25	2.5	529	1082	1298	811	300	617	-2.15	-1.14	184	621
24	1	0.5	6.25	2.5	531	1098	1519	665	300	615	-2.40	-1.20	183	603
25	100	0.1	6.25	2.5	513	1018	1035	993	300	621	-0.49	-0.35	179	669
26	10	0.1	6.25	2.5	513	1022	1114	884	300	621	-0.49	-0.36	178	664
27	1	0.1	3.125	2.5	515	1042	1310	763	300	621	-0.51	-0.42	177	641
28	100	0.9	3.125	2.5	700	1366	1533	1231	300	861	-6.65	-3.87	83	485
29	10	0.9	3.125	2.5	703	1370	1668	975	300	852	-8.16	-3.31	83	476

Continued on next page

Table B.2 – 2^3 *Cells Parametric Study Results Continued ...*

N	k_s	ϵ	m''	G	$\overline{T}_g$	$\overline{T}_s$	$T_{s,max}$	$T_{s,min}$	T_{in}	T_{out}	$q_{rad,in}$	$q_{rad,out}$	ΔP	h_v
	$\frac{W}{m \cdot K}$		$\frac{kg}{m^2 \cdot s}$	$\frac{MW}{m^2}$	K	K	K	K	K	K	W	W	Pa	$\frac{kW}{m^3 \cdot K}$
30	1	0.9	3.125	2.5	700	1375	1914	750	300	843	-9.43	-3.10	82	462
31	100	0.5	3.125	2.5	699	1325	1386	1244	300	887	-4.03	-2.59	82	520
32	10	0.5	3.125	2.5	702	1333	1509	1038	300	884	-4.50	-2.43	83	513
33	1	0.5	3.125	2.5	704	1348	1712	838	300	880	-4.83	-2.51	82	499
34	100	0.1	3.125	2.5	693	1288	1324	1255	300	910	-1.37	-0.65	82	557
35	10	0.1	3.125	2.5	692	1290	1453	1125	300	910	-1.33	-0.70	81	554
36	1	0.1	1.25	2.5	695	1309	1728	926	300	908	-1.36	-0.85	80	538
37	100	0.9	1.25	2.5	515	777	972	538	300	614	-0.77	-0.22	12	270
38	10	0.9	1.25	2.5	513	770	865	653	300	616	-0.68	-0.23	12	277
39	1	0.9	1.25	2.5	509	763	790	737	300	618	-0.58	-0.26	12	283
40	100	0.5	1.25	2.5	506	745	847	561	300	620	-0.40	-0.14	12	290
41	10	0.5	1.25	2.5	505	739	778	667	300	621	-0.38	-0.13	12	297
42	1	0.5	1.25	2.5	504	736	744	724	300	621	-0.37	-0.13	12	300
43	100	0.1	1.25	2.5	681	1105	1383	742	300	863	-3.18	-0.92	19	307
44	10	0.1	1.25	2.5	682	1098	1236	906	300	870	-2.86	-0.96	19	315
45	1	0.1	12.5	2.5	495	709	898	565	300	624	-0.15	0.00	11	317
46	100	0.9	12.5	2	394	782	932	669	300	434	-0.81	-0.41	452	768
47	10	0.9	12.5	2	399	787	1169	524	300	433	-1.26	-0.35	455	762
48	1	0.9	12.5	2	399	791	1390	435	300	432	-1.66	-0.34	455	750
49	100	0.5	12.5	2	388	740	823	671	300	433	-0.41	-0.27	443	811
50	10	0.5	12.5	2	391	745	973	568	300	433	-0.53	-0.24	445	804
51	1	0.5	12.5	2	392	754	1131	498	300	432	-0.62	-0.25	444	786
52	100	0.1	12.5	2	381	697	715	675	300	431	-0.11	-0.08	433	865
53	10	0.1	12.5	2	382	700	774	614	300	431	-0.11	-0.08	433	858
54	1	0.1	9.375	2	383	712	905	562	300	431	-0.11	-0.08	432	830
55	100	0.9	9.375	2	427	863	1009	747	300	476	-1.17	-0.63	292	676
56	10	0.9	9.375	2	432	869	1238	580	300	475	-1.76	-0.52	294	669
57	1	0.9	9.375	2	433	875	1456	472	300	473	-2.25	-0.52	294	655
58	100	0.5	9.375	2	419	817	897	747	300	476	-0.61	-0.41	286	713
59	10	0.5	9.375	2	422	823	1041	627	300	475	-0.77	-0.37	287	706

Continued on next page

Table B.2 – 2^3 *Cells Parametric Study Results Continued ...*

N	k_s	ϵ	m''	G	$\overline{T}_g$	$\overline{T}_s$	$T_{s,max}$	$T_{s,min}$	T_{in}	T_{out}	$q_{rad,in}$	$q_{rad,out}$	ΔP	h_v
	$\frac{W}{m \cdot K}$		$\frac{kg}{m^2 \cdot s}$	$\frac{MW}{m^2}$	K	K	K	K	K	K	W	W	Pa	$\frac{kW}{m^3 \cdot K}$
60	1	0.5	9.375	2	424	834	1218	540	300	475	-0.88	-0.38	287	689
61	100	0.1	9.375	2	411	770	787	748	300	475	-0.16	-0.11	279	760
62	10	0.1	9.375	2	411	773	852	678	300	475	-0.16	-0.11	279	754
63	1	0.1	6.25	2	413	787	992	611	300	475	-0.17	-0.13	278	729
64	100	0.9	6.25	2	490	991	1126	875	300	557	-1.94	-1.13	165	574
65	10	0.9	6.25	2	496	998	1335	675	300	554	-2.73	-0.94	167	567
66	1	0.9	6.25	2	496	1005	1560	527	300	551	-3.36	-0.92	166	553
67	100	0.5	6.25	2	481	942	1011	873	300	559	-1.05	-0.73	162	607
68	10	0.5	6.25	2	485	949	1140	726	300	558	-1.27	-0.66	163	600
69	1	0.5	6.25	2	487	963	1333	604	300	557	-1.42	-0.70	162	583
70	100	0.1	6.25	2	471	891	905	872	300	560	-0.29	-0.20	158	646
71	10	0.1	6.25	2	471	894	971	785	300	560	-0.29	-0.20	158	641
72	1	0.1	3.125	2	473	911	1128	686	300	560	-0.30	-0.24	157	619
73	100	0.9	3.125	2	636	1214	1328	1101	300	771	-4.11	-2.42	72	465
74	10	0.9	3.125	2	640	1219	1496	874	300	765	-5.17	-2.06	73	457
75	1	0.9	3.125	2	639	1226	1717	669	300	758	-6.03	-1.95	72	444
76	100	0.5	3.125	2	632	1170	1222	1105	300	787	-2.44	-1.58	71	496
77	10	0.5	3.125	2	635	1178	1334	928	300	785	-2.75	-1.48	72	490
78	1	0.5	3.125	2	637	1192	1518	747	300	782	-2.97	-1.54	71	477
79	100	0.1	3.125	2	624	1129	1158	1101	300	801	-0.81	-0.38	70	531
80	10	0.1	3.125	2	624	1130	1266	998	300	801	-0.78	-0.41	70	528
81	1	0.1	1.25	2	626	1146	1507	827	300	800	-0.80	-0.50	69	513
82	100	0.9	1.25	2	498	710	725	694	300	625	-0.15	0.01	11	320
83	10	0.9	1.25	2	678	1091	1137	1042	300	875	-2.49	-1.07	19	322
84	1	0.9	1.25	2	496	706	777	639	300	625	-0.15	0.01	11	323
85	100	0.5	1.25	2	812	1352	1675	924	300	1061	-7.02	-2.04	24	331
86	10	0.5	1.25	2	679	1075	1255	780	300	894	-1.75	-0.58	18	333
87	1	0.5	1.25	2	813	1346	1506	1103	300	1063	-6.39	-2.24	24	336
88	100	0.1	1.25	2	679	1067	1128	940	300	896	-1.69	-0.54	18	341
89	10	0.1	1.25	2	915	1547	1915	1078	300	1212	-11.94	-3.58	29	343

Continued on next page

Table B.2 – 2^3 *Cells Parametric Study Results Continued ...*

N	k_s	ϵ	m''	G	$\overline{T}_g$	$\overline{T}_s$	$T_{s,max}$	$T_{s,min}$	T_{in}	T_{out}	$q_{rad,in}$	$q_{rad,out}$	ΔP	h_v
	$\frac{W}{m \cdot K}$		$\frac{kg}{m^2 \cdot s}$	$\frac{MW}{m^2}$	K	K	K	K	K	K	W	W	Pa	$\frac{kW}{m^3 \cdot K}$
90	1	0.1	12.5	2	810	1340	1447	1271	300	1073	-5.72	-2.48	24	343
91	100	0.9	12.5	1.5	370	670	786	585	300	401	-0.42	-0.22	409	749
92	10	0.9	12.5	1.5	374	675	988	473	300	401	-0.64	-0.18	411	742
93	1	0.9	12.5	1.5	374	679	1175	404	300	400	-0.84	-0.18	411	733
94	100	0.5	12.5	1.5	365	637	701	586	300	400	-0.22	-0.14	401	791
95	10	0.5	12.5	1.5	367	641	823	507	300	400	-0.28	-0.13	403	784
96	1	0.5	12.5	1.5	368	648	950	452	300	400	-0.32	-0.13	402	768
97	100	0.1	12.5	1.5	361	604	617	587	300	399	-0.06	-0.04	394	843
98	10	0.1	12.5	1.5	361	606	659	542	300	399	-0.06	-0.04	394	837
99	1	0.1	9.375	1.5	362	614	758	502	300	399	-0.06	-0.04	392	811
100	100	0.9	9.375	1.5	394	735	850	647	300	434	-0.59	-0.33	259	655
101	10	0.9	9.375	1.5	399	741	1051	517	300	433	-0.90	-0.27	262	649
102	1	0.9	9.375	1.5	400	746	1237	433	300	432	-1.15	-0.27	261	638
103	100	0.5	9.375	1.5	388	698	760	645	300	433	-0.32	-0.21	255	692
104	10	0.5	9.375	1.5	391	703	882	554	300	433	-0.39	-0.19	256	685
105	1	0.5	9.375	1.5	392	711	1019	486	300	433	-0.45	-0.19	255	669
106	100	0.1	9.375	1.5	382	660	673	644	300	432	-0.09	-0.06	249	737
107	10	0.1	9.375	1.5	383	663	722	593	300	432	-0.09	-0.06	249	732
108	1	0.1	6.25	1.5	384	673	833	541	300	432	-0.09	-0.06	248	709
109	100	0.9	6.25	1.5	443	842	949	752	300	497	-0.99	-0.58	143	552
110	10	0.9	6.25	1.5	449	849	1139	594	300	495	-1.41	-0.48	145	546
111	1	0.9	6.25	1.5	450	856	1330	479	300	494	-1.76	-0.47	145	533
112	100	0.5	6.25	1.5	436	800	854	747	300	497	-0.54	-0.37	140	583
113	10	0.5	6.25	1.5	439	806	966	635	300	497	-0.65	-0.34	141	577
114	1	0.5	6.25	1.5	441	817	1123	540	300	496	-0.73	-0.35	141	561
115	100	0.1	6.25	1.5	428	756	767	743	300	497	-0.15	-0.10	137	621
116	10	0.1	6.25	1.5	428	759	819	679	300	497	-0.15	-0.10	137	616
117	1	0.1	3.125	1.5	429	772	933	603	300	497	-0.16	-0.11	136	596
118	100	0.9	3.125	1.5	565	1039	1130	951	300	670	-2.18	-1.30	61	442
119	10	0.9	3.125	1.5	569	1046	1292	762	300	666	-2.82	-1.10	61	434

Continued on next page

Table B.2 – 2^3 *Cells Parametric Study Results Continued ...*

N	k_s	ϵ	m''	G	$\overline{T}_g$	$\overline{T}_s$	$T_{s,max}$	$T_{s,min}$	T_{in}	T_{out}	$q_{rad,in}$	$q_{rad,out}$	ΔP	h_v
	$\frac{W}{m \cdot K}$		$\frac{kg}{m^2 \cdot s}$	$\frac{MW}{m^2}$	K	K	K	K	K	K	W	W	Pa	$\frac{kW}{m^3 \cdot K}$
120	1	0.9	3.125	1.5	570	1053	1485	586	300	662	-3.32	-1.06	61	423
121	100	0.5	3.125	1.5	558	997	1037	947	300	678	-1.27	-0.83	59	469
122	10	0.5	3.125	1.5	561	1004	1133	804	300	677	-1.44	-0.77	60	463
123	1	0.5	3.125	1.5	563	1016	1293	651	300	675	-1.56	-0.81	60	451
124	100	0.1	3.125	1.5	550	955	976	933	300	685	-0.41	-0.19	58	500
125	10	0.1	3.125	1.5	549	956	1061	847	300	685	-0.40	-0.21	58	498
126	1	0.1	1.25	1.5	551	969	1260	720	300	685	-0.41	-0.25	57	484
127	100	0.9	1.25	1.5	677	1062	1075	1041	300	897	-1.64	-0.54	18	345
128	10	0.9	1.25	1.5	1002	1712	2124	1221	300	1346	-17.76	-5.27	32	354
129	1	0.9	1.25	1.5	921	1545	1716	1267	300	1228	-10.97	-3.84	29	354
130	100	0.5	1.25	1.5	920	1540	1662	1455	300	1238	-10.02	-4.23	29	361
131	10	0.5	1.25	1.5	824	1338	1572	980	300	1125	-4.17	-1.28	24	364
132	1	0.5	1.25	1.5	1009	1711	1890	1408	300	1363	-16.38	-5.78	32	365
133	100	0.1	1.25	1.5	671	1035	1359	771	300	920	-0.69	0.05	18	367
134	10	0.1	1.25	1.5	677	1038	1068	1001	300	921	-0.74	0.11	18	371
135	1	0.1	12.5	1.5	1010	1708	1844	1608	300	1377	-15.18	-6.32	32	372
136	100	0.9	12.5	1	346	554	633	496	300	368	-0.18	-0.10	363	726
137	10	0.9	12.5	1	349	558	785	419	300	368	-0.26	-0.08	366	720
138	1	0.9	12.5	1	349	560	926	371	300	368	-0.34	-0.08	366	714
139	100	0.5	12.5	1	343	531	587	496	300	367	-0.10	-0.06	358	767
140	10	0.5	12.5	1	344	533	662	442	300	367	-0.12	-0.06	359	760
141	1	0.5	12.5	1	345	537	752	404	300	367	-0.14	-0.06	359	747
142	100	0.1	12.5	1	340	507	533	483	300	366	-0.03	-0.02	353	819
143	10	0.1	12.5	1	340	508	544	466	300	366	-0.03	-0.02	353	813
144	1	0.1	9.375	1	341	514	607	438	300	366	-0.03	-0.02	352	789
145	100	0.9	9.375	1	362	600	679	541	300	390	-0.25	-0.14	226	632
146	10	0.9	9.375	1	366	605	836	451	300	390	-0.36	-0.11	228	626
147	1	0.9	9.375	1	367	608	981	392	300	390	-0.46	-0.11	228	618
148	100	0.5	9.375	1	358	574	616	538	300	389	-0.14	-0.09	222	667
149	10	0.5	9.375	1	360	577	707	476	300	389	-0.17	-0.08	223	661

Continued on next page

Table B.2 – 2^3 *Cells Parametric Study Results Continued ...*

N	k_s	ϵ	m''	G	$\overline{T}_g$	$\overline{T}_s$	$T_{s,max}$	$T_{s,min}$	T_{in}	T_{out}	$q_{rad,in}$	$q_{rad,out}$	ΔP	h_v
	$\frac{W}{m \cdot K}$		$\frac{kg}{m^2 \cdot s}$	$\frac{MW}{m^2}$	K	K	K	K	K	K	W	W	Pa	$\frac{kW}{m^3 \cdot K}$
150	1	0.5	9.375	1	361	582	802	429	300	389	-0.19	-0.08	223	647
151	100	0.1	9.375	1	354	547	555	536	300	388	-0.04	-0.02	218	711
152	10	0.1	9.375	1	355	548	588	502	300	388	-0.04	-0.02	218	706
153	1	0.1	6.25	1	355	555	665	467	300	388	-0.04	-0.03	218	685
154	100	0.9	6.25	1	395	678	753	617	300	434	-0.40	-0.23	120	527
155	10	0.9	6.25	1	399	684	909	507	300	433	-0.57	-0.19	121	521
156	1	0.9	6.25	1	401	690	1055	427	300	433	-0.71	-0.19	122	511
157	100	0.5	6.25	1	390	646	685	611	300	433	-0.22	-0.15	118	556
158	10	0.5	6.25	1	392	651	772	535	300	433	-0.26	-0.13	119	551
159	1	0.5	6.25	1	393	658	885	469	300	433	-0.30	-0.14	119	537
160	100	0.1	6.25	1	384	615	622	606	300	432	-0.07	-0.04	116	592
161	10	0.1	6.25	1	384	616	657	564	300	432	-0.07	-0.04	115	588
162	1	0.1	3.125	1	385	625	740	513	300	432	-0.07	-0.04	115	570
163	100	0.9	3.125	1	484	835	901	775	300	558	-0.89	-0.54	48	411
164	10	0.9	3.125	1	489	843	1042	634	300	556	-1.17	-0.45	49	405
165	1	0.9	3.125	1	490	850	1197	500	300	554	-1.40	-0.44	49	395
166	100	0.5	3.125	1	477	799	828	766	300	560	-0.52	-0.33	47	435
167	10	0.5	3.125	1	480	805	900	665	300	560	-0.59	-0.31	47	430
168	1	0.5	3.125	1	482	815	1026	550	300	559	-0.64	-0.33	47	419
169	100	0.1	3.125	1	470	763	778	748	300	562	-0.17	-0.07	46	463
170	10	0.1	3.125	1	470	764	836	701	300	562	-0.16	-0.08	45	461
171	1	0.1	1.25	1	471	773	979	602	300	562	-0.16	-0.09	45	448
172	100	0.9	1.25	1	821	1322	1388	1256	300	1122	-3.95	-1.30	24	372
173	10	0.9	1.25	1	825	1329	1401	1165	300	1129	-4.06	-1.18	24	373
174	1	0.9	1.25	1	672	1030	1164	902	300	921	-0.70	0.09	18	374
175	100	0.5	1.25	1	947	1555	1831	1166	300	1324	-7.59	-2.11	29	388
176	10	0.5	1.25	1	945	1543	1628	1349	300	1319	-7.35	-2.22	30	393
177	1	0.5	1.25	1	944	1538	1558	1500	300	1319	-7.24	-2.23	30	395
178	100	0.1	1.25	1	1046	1738	2046	1321	300	1482	-11.77	-3.45	33	398
179	10	0.1	1.25	1	827	1315	1728	946	300	1186	-1.86	0.25	24	403

Continued on next page

Table B.2 – 2^3 *Cells Parametric Study Results Continued ...*

N	k_s	ϵ	m''	G	$\overline{T}_g$	$\overline{T}_s$	$T_{s,max}$	$T_{s,min}$	T_{in}	T_{out}	$q_{rad,in}$	$q_{rad,out}$	ΔP	h_v
	$\frac{W}{m\cdot K}$		$\frac{kg}{m^2\cdot s}$	$\frac{MW}{m^2}$	K	K	K	K	K	K	W	W	Pa	$\frac{kW}{m^3\cdot K}$
180	1	0.1	12.5	1	1048	1728	1825	1514	300	1487	-11.52	-3.37	34	407
181	100	0.9	12.5	0.5	323	431	471	402	300	334	-0.05	-0.03	317	701
182	10	0.9	12.5	0.5	324	433	557	361	300	334	-0.07	-0.02	318	694
183	1	0.9	12.5	0.5	324	434	637	336	300	334	-0.09	-0.02	318	690
184	100	0.5	12.5	0.5	321	418	440	401	300	334	-0.03	-0.02	314	742
185	10	0.5	12.5	0.5	322	420	489	373	300	334	-0.04	-0.02	314	736
186	1	0.5	12.5	0.5	322	422	538	354	300	334	-0.04	-0.02	314	724
187	100	0.1	12.5	0.5	320	406	410	401	300	333	-0.01	0.00	311	795
188	10	0.1	12.5	0.5	320	406	423	386	300	333	-0.01	0.00	311	789
189	1	0.1	9.375	0.5	320	409	454	371	300	333	-0.01	-0.01	310	767
190	100	0.9	9.375	0.5	331	456	497	426	300	346	-0.07	-0.04	191	603
191	10	0.9	9.375	0.5	332	459	589	379	300	346	-0.09	-0.03	192	597
192	1	0.9	9.375	0.5	333	460	674	348	300	345	-0.11	-0.03	192	592
193	100	0.5	9.375	0.5	329	441	463	424	300	345	-0.04	-0.03	189	638
194	10	0.5	9.375	0.5	330	443	515	392	300	345	-0.05	-0.02	189	632
195	1	0.5	9.375	0.5	330	446	568	367	300	345	-0.05	-0.02	189	621
196	100	0.1	9.375	0.5	327	427	431	422	300	344	-0.01	-0.01	187	683
197	10	0.1	9.375	0.5	327	428	447	405	300	344	-0.01	-0.01	187	678
198	1	0.1	6.25	0.5	327	431	485	387	300	344	-0.01	-0.01	186	659
199	100	0.9	6.25	0.5	347	499	539	468	300	368	-0.10	-0.06	96	495
200	10	0.9	6.25	0.5	349	503	635	410	300	368	-0.14	-0.05	97	490
201	1	0.9	6.25	0.5	350	505	725	368	300	368	-0.17	-0.05	97	483
202	100	0.5	6.25	0.5	344	481	502	464	300	367	-0.06	-0.04	95	523
203	10	0.5	6.25	0.5	345	484	554	425	300	367	-0.07	-0.03	95	518
204	1	0.5	6.25	0.5	346	487	614	390	300	367	-0.08	-0.03	95	507
205	100	0.1	6.25	0.5	341	464	468	460	300	367	-0.02	-0.01	94	558
206	10	0.1	6.25	0.5	342	465	486	440	300	367	-0.02	-0.01	94	555
207	1	0.1	3.125	0.5	342	469	531	413	300	367	-0.02	-0.01	93	539
208	100	0.9	3.125	0.5	394	594	629	564	300	434	-0.21	-0.13	34	372
209	10	0.9	3.125	0.5	397	600	723	486	300	433	-0.27	-0.10	35	367

Continued on next page

Table B.2 – 2^3 *Cells Parametric Study Results Continued ...*

N	k_s	ϵ	m''	G	$\overline{T}_g$	$\overline{T}_s$	$T_{s,max}$	$T_{s,min}$	T_{in}	T_{out}	$q_{rad,in}$	$q_{rad,out}$	ΔP	h_v
	$\frac{W}{m \cdot K}$		$\frac{kg}{m^2 \cdot s}$	$\frac{MW}{m^2}$	K	K	K	K	K	K	W	W	Pa	$\frac{kW}{m^3 \cdot K}$
210	1	0.9	3.125	0.5	399	605	821	410	300	433	-0.32	-0.10	35	359
211	100	0.5	3.125	0.5	390	572	587	555	300	433	-0.13	-0.08	34	392
212	10	0.5	3.125	0.5	391	575	631	502	300	433	-0.14	-0.07	34	388
213	1	0.5	3.125	0.5	393	580	705	439	300	433	-0.15	-0.07	34	379
214	100	0.1	3.125	0.5	386	549	556	542	300	433	-0.04	-0.02	33	418
215	10	0.1	3.125	0.5	385	549	584	517	300	433	-0.04	-0.02	33	416
216	1	0.1	1.25	0.5	386	554	656	468	300	433	-0.04	-0.02	33	405
217	100	0.9	1.25	0.5	836	1319	1365	1208	300	1188	-1.98	0.42	25	408
218	10	0.9	1.25	0.5	1048	1724	1798	1622	300	1490	-11.44	-3.33	34	410
219	1	0.9	1.25	0.5	829	1308	1496	1095	300	1189	-1.88	0.37	24	412
220	100	0.5	1.25	0.5	962	1561	2033	1101	300	1425	-3.78	0.67	29	429
221	10	0.5	1.25	0.5	976	1567	1629	1505	300	1428	-4.06	1.09	31	436
222	1	0.5	1.25	0.5	966	1554	1789	1318	300	1430	-3.83	0.95	30	439
223	100	0.1	1.25	0.5	1083	1788	2293	1243	300	1643	-6.57	1.35	34	445
224	10	0.1	1.25	0.5	1098	1796	1873	1718	300	1647	-7.05	2.03	36	452
225	1	0.1	1.25	0.5	1088	1781	2058	1495	300	1650	-6.69	1.81	35	456
226	100	0.9	3.125	0	300	300	300	300	300	300	0.00	0.00	4	-
227	100	0.9	6.25	0	300	300	300	300	300	300	0.00	0.00	20	-
228	100	0.9	9.375	0	300	300	300	300	300	300	0.00	0.00	71	-
229	100	0.9	12.5	0	300	300	300	300	300	300	0.00	0.00	155	-
230	100	0.9	1.25	0	300	300	300	300	300	300	0.00	0.00	268	-

REFERENCES

[1] G. Zulhazmi, “Absorber Materials for Solar Thermal Power Plant,” Master’s thesis, KFUPM.

[2] Z. Wu, C. Caliot, F. Bai, G. Flamant, Z. Wang, J. Zhang, and C. Tian, “Experimental and numerical studies of the pressure drop in ceramic foams for volumetric solar receiver applications,” *Applied Energy*, vol. 87, no. 2, pp. 504–513, 2010.

[3] L. Younis and R. Viskanta, “Experimental determination of the volumetric heat transfer coefficient between stream of air and ceramic foam,” *International Journal of Heat and Mass Transfer*, vol. 36, no. 6, pp. 1425–1434, jan 1993.

[4] T. J. Hendricks, “Thermal Radiative Properties and Modelling of Reticulated Porous Ceramics,” Ph.D. dissertation, 1993.

[5] Z. Wu, C. Caliot, G. Flamant, and Z. Wang, “Numerical simulation of convective heat transfer between air flow and ceramic foams to optimise volu-

metric solar air receiver performances," *International Journal of Heat and Mass Transfer*, vol. 54, no. 7-8, pp. 1527–1537, 2011.

[6] G. L. Vignoles and A. Ortona, "Numerical study of effective heat conductivities of foams by coupled conduction and radiation," *International Journal of Thermal Sciences*, vol. 109, pp. 270–278, 2016.

[7] REN21, *Renewables 2016 Global Status Report*, 2016. [Online]. Available: http://www.ren21.net/status-of-renewables/global-status-report/

[8] N. Dukhan, Ö. Baci, and M. Özdemir, "Experimental flow in various porous media and reconciliation of Forchheimer and Ergun relations," *Experimental Thermal and Fluid Science*, vol. 57, pp. 425–433, 2014.

[9] "Fluent Userguide 6.1. Lebanon." 2006.

[10] B. Dietrich, "Heat transfer coefficients for solid ceramic sponges-Experimental results and correlation," *International Journal of Heat and Mass Transfer*, vol. 61, no. 1, pp. 627–637, 2013.

[11] S. Brendelberger, S. Hötker, T. Fend, and R. Pitz-Paal, "Macroscopic foam model with effective material properties for high heat load applications," *Applied Thermal Engineering*, vol. 47, pp. 34–40, 2012.

[12] M. A. Mendes, P. Goetze, P. Talukdar, E. Werzner, C. Demuth, P. Rössger, R. Wulf, U. Gross, D. Trimis, and S. Ray, "Measurement and simplified numerical prediction of effective thermal conductivity of open-cell ceramic foams

at high temperature," *International Journal of Heat and Mass Transfer*, vol. 102, pp. 396–406, 2016.

[13] R. Coquard and D. Baillis, "Numerical investigation of conductive heat transfer in high-porosity foams," *Acta Materialia*, vol. 57, no. 18, pp. 5466–5479, 2009.

[14] M. Wallenstein, M. Kind, and B. Dietrich, "Radial two-phase thermal conductivity and wall heat transfer coefficient of ceramic sponges - Experimental results and correlation," *International Journal of Heat and Mass Transfer*, vol. 79, pp. 486–495, 2014.

[15] B. Dietrich, M. Kind, and H. Martin, "Axial two-phase thermal conductivity of ceramic sponges - Experimental results and correlation," *International Journal of Heat and Mass Transfer*, vol. 54, no. 11-12, pp. 2276–2282, 2011.

[16] B. R. Galen, "Information to users," 2003.

[17] M. Hale and M. Bohn, "Measurement of the radiative transport properties of reticulated alumina foams," *Conference: SOLAR '93: American Society of Mechanical Engineers (ASME)/American Solar Energy Society (ASES) joint solar energy conference*, 1992.

[18] C. Y. Zhao, T. J. Lu, and H. P. Hodson, "Thermal radiation in ultralight metal foams with open cells," *International Journal of Heat and Mass Transfer*, vol. 47, no. 14-16, pp. 2927–2939, 2004.

[19] "A model for the volumetric radiation characteristics of cellular ceramics," *International Communications in Heat and Mass Transfer*, vol. 24, no. 8, pp. 1069–1082, 1997.

[20] S. Krishnan, J. Y. Murthy, and S. V. Garimella, "Direct Simulation of Transport in Open-Cell Metal Foam," *Journal of Heat Transfer*, vol. 128, no. 8, p. 793, 2006.

[21] A. Andreozzi, N. Bianco, O. Manca, and V. Naso, "Numerical analysis of radiation effects in a metallic foam by means of the radiative conductivity model," *Applied Thermal Engineering*, vol. 49, pp. 14–21, 2012.

[22] R. Coquard, D. Rochais, and D. Baillis, "Experimental investigations of the coupled conductive and radiative heat transfer in metallic/ceramic foams," *International Journal of Heat and Mass Transfer*, vol. 52, no. 21-22, pp. 4907–4918, 2009.

[23] X. H. Yang, J. X. Bai, H. B. Yan, J. J. Kuang, T. J. Lu, and T. Kim, "An Analytical Unit Cell Model for the Effective Thermal Conductivity of High Porosity Open-Cell Metal Foams," *Transport in Porous Media*, vol. 102, no. 3, pp. 403–426, 2014.

[24] Y. Yao, H. Wu, and Z. Liu, "A new prediction model for the effective thermal conductivity of high porosity open-cell metal foams," *International Journal of Thermal Sciences*, vol. 97, pp. 56–67, 2015.

[25] J. E. Li and B. Wang, “Equivalent thermal conductivity of open-cell ceramic foams at high temperatures,” *International Journal of Thermophysics*, vol. 35, no. 1, pp. 105–122, 2014.

[26] S. Guévelou, B. Rousseau, G. Domingues, J. Vicente, and C. Caliot, “Representative elementary volumes required to characterize the normal spectral emittance of silicon carbide foams used as volumetric solar absorbers,” *International Journal of Heat and Mass Transfer*, vol. 93, pp. 118–129, 2016.

[27] M. Becker, T. Fend, B. Hoffschmidt, R. Pitz-Paal, O. Reutter, V. Stamatov, M. Steven, and D. Trimis, “Theoretical and numerical investigation of flow stability in porous materials applied as volumetric solar receivers,” *Solar Energy*, vol. 80, no. 10, pp. 1241–1248, 2006.

[28] J. Natividade, “Parametric Study of High-Temperature Volumetric Solar Absorbers,” 2015.

[29] T. Fend, R. Pitz-Paal, O. Reutter, J. ö. Bauer, and B. Hoffschmidt, “Two novel high-porosity materials as volumetric receivers for concentrated solar radiation,” *Solar Energy Materials and Solar Cells*, vol. 84, no. 1-4, pp. 291–304, 2004.

[30] T. P. Otanicar, P. E. Phelan, R. A. Taylor, and H. Tyagi, “Spatially Varying Extinction Coefficient for Direct Absorption Solar Thermal Collector Optimization,” *Journal of Solar Energy Engineering*, vol. 133, no. 2, p. 024501, 2011.

[31] “Evaluation of porous silicon carbide monolithic honeycombs as volumetric receivers/collectors of concentrated solar radiation,” *Solar Energy Materials and Solar Cells*, vol. 91, no. 6, pp. 474–488, 2007.

[32] G. Contento, M. Oliviero, N. Bianco, and V. Naso, “Prediction of radiative heat transfer in metallic foams,” *International Journal of Thermal Sciences*, vol. 76, pp. 147–154, 2014.

[33] C. Y. Zhao, S. A. Tassou, and T. J. Lu, “Analytical considerations of thermal radiation in cellular metal foams with open cells,” *International Journal of Heat and Mass Transfer*, vol. 51, no. 3-4, pp. 929–940, 2008.

[34] M. Wang and N. Pan, “Modeling and prediction of the effective thermal conductivity of random open-cell porous foams,” *International Journal of Heat and Mass Transfer*, vol. 51, no. 5-6, pp. 1325–1331, 2008.

[35] T. Fend, B. Hoffschmidt, R. Pitz-Paal, O. Reutter, and P. Rietbrock, “Porous materials as open volumetric solar receivers: Experimental determination of thermophysical and heat transfer properties,” *Energy*, vol. 29, no. 5-6, pp. 823–833, 2004.

[36] P. Wang, K. Vafai, and D. Y. Liu, “Analysis of radiative effect under local thermal non-equilibrium conditions in porous media-application to a solar air receiver,” *Numerical Heat Transfer; Part A: Applications*, vol. 65, no. 10, pp. 931–948, 2014.

[37] R. Bertocchi, J. Karni, and A. Kribus, "Experimental evaluation of a non-isothermal high temperature solar particle receiver," *Energy*, vol. 29, no. 5-6, pp. 687–700, 2004.

[38] S. Mey-Cloutier, C. Caliot, A. Kribus, Y. Gray, and G. Flamant, "Experimental study of ceramic foams used as high temperature volumetric solar absorber," *Solar Energy*, vol. 136, pp. 226–235, 2016.

[39] M. Kaviany, "Principles of Heat Transfer in Porous Media," *Mechanical Engineering Series*, vol. 53, no. 9, p. 726, 1995.

Vitae

- Name: Majid Tareq Linjawi
- Nationality: Saudi
- Date of Birth: 25,April,1991
- Email:

  mlinjawi@kfupm.edu.sa

  mlinjawi@gmail.com

- Permenant Address:

  3504 Abdul Rahman At Tunsi
  Ash Shati District
  Jeddah 23513-7636
  Saudi Arabia

- Bachelor of Science In Mechanical Engineering, 2015 KFUPM
- Master's of Science In Mechanical Engineering - Thermo-fluids, 2018 KFUPM